Hunting for dark matter coannihilation by mixing dijet resonances and missing transverse energy

Malte Buschmann,[a] **Sonia El Hedri,**[a] **Anna Kaminska,**[a] **Jia Liu,**[a] **Maikel de Vries,**[a] **Xiao-Ping Wang,**[a] **Felix Yu**[a] **and José Zurita**[b,c]

[a]*PRISMA Cluster of Excellence & Mainz Institute for Theoretical Physics,*
Johannes Gutenberg University,
55099 Mainz, Germany

[b]*Institute for Theoretical Physics (ITP), Karlsruhe Institute of Technology,*
Engesserstraße 7, D-76128 Karlsruhe, Germany

[c]*Institute for Nuclear Physics (IKP), Karlsruhe Institute of Technology,*
Hermann-von-Helmholtz-Platz 1, D-76344 Eggenstein-Leopoldshafen, Germany

E-mail: buschman@uni-mainz.de, elhed001@uni-mainz.de,
akaminsk@uni-mainz.de, liuj@uni-mainz.de, mdevrie@uni-mainz.de,
xiaowang@uni-mainz.de, yu001@uni-mainz.de, jose.zurita@kit.edu

ABSTRACT: Simplified models of the dark matter (co)annihilation mechanism predict striking new collider signatures untested by current searches. These models, which were codified in the coannihilation codex, provide the basis for a dark matter (DM) discovery program at the Large Hadron Collider (LHC) driven by the measured DM relic density. In this work, we study an exemplary model featuring s-channel DM coannihilation through a scalar diquark mediator as a representative case study of scenarios with strongly interacting coannihilation partners. We discuss the full phenomenology of the model, ranging from low energy flavor constraints, vacuum stability requirements, and precision Higgs effects to direct detection and indirect detection prospects. Moreover, motivated by the relic density calculation, we find significant portions of parameter space are compatible with current collider constraints and can be probed by future searches, including a proposed analysis for the novel signature of a dijet resonance accompanied by missing transverse energy (MET). Our results show that the 13 TeV LHC with 100 fb^{-1} luminosity should be sensitive to mediators as heavy as 1 TeV and dark matter in the 400–500 GeV range. The combination of searches for single and paired dijet peaks, non-resonant jets + MET excesses, and our novel resonant dijet + MET signature have strong coverage of the motivated relic density region, reflecting the tight connections between particles determining the dark matter abundance and their experimental signatures at the LHC.

Contents

1 Introduction

With the resumption of the Large Hadron Collider (LHC) operating at $\sqrt{s} = 13\,\text{TeV}$, the hunt for collider signals of dark matter (DM) production has again begun in earnest. A positive signal of dark matter at the LHC would spur a revolution in particle physics and astrophysics, although the huge breadth of dark matter models and their concomitant collider signatures makes designing a search strategy a daunting task. In particular, most of our current knowledge voids possible interactions of the DM, rendering it colorless and electrically neutral, while the only concrete DM measurement is its relic density, $\Omega h^2 = 0.1198 \pm 0.0026$ [1, 2].

Nevertheless, the relic density requirement has not featured prominently in collider searches thus far. In particular, the dark matter relic density can be driven by all interactions of dark sector particles, while collider searches based on effective operators [3–7] or dark matter pair annihilation simplified models [8–16] eschew such complications. As a

result, the collider searches for dark matter are mainly variations on a theme of missing transverse energy [17–22] instead of being driven by the known dark matter relic density.

In reference [23], we established a bottom-up framework for dark matter discovery at the LHC based on a simplified model treatment of the (co)annihilation mechanism of thermal relic dark matter. This approach uncovered several new signatures ripe for analysis, and more importantly, ensures a direct connection between the relic density calculation and the collider signatures associated with the model. One novelty with this construction was the inclusion of DM coannihilation [24] in addition to pair annihilation, as the mere presence of the coannihilation partner together with the mediator radically adds to the complexity and variety of DM collider signatures. We stress that, unlike the dark matter field, the coannihilating partner and the mediator of the coannihilation diagram can have color and electromagnetic charges. In this way, the collider signatures of the dark matter, coannihilation partner, and the mediator are driven by production and decay modes dictated by the coannihilation codex [23].

Because the relic density measurement motivates the simplified model construction, we use the Ωh^2 calculation to inform the most promising parameter space for a dark matter discovery at the LHC. In this way, naive expectations about DM phenomenology from the weakly-interacting massive particle (WIMP) miracle (see reference [25] for a review) are sharpened into concrete predictions for dark sector particle masses and couplings with real discovery prospects at the LHC. Our approach also complements the broader community efforts at exploring non-WIMP phenomenology at colliders (see, e.g., references [26–30]).

In this work, we continue our exploration of the models presented in the codex, again focusing on the case when the coannihilation partner and the s-channel mediator are colored particles. In contrast with the s-channel leptoquark case study presented in reference [23], though, we study an s-channel diquark mediator with Yukawa couplings to first generation quarks. Since the dark matter pair annihilation rate is suppressed, the DM relic density will mainly be set by processes involving only strong interactions. As a result, the dark sector mass scale can be readily estimated for a wide range of strongly interacting models which depend only on the $\text{SU}(3)_C$ representation of the coannihilation partner and its relative splitting with the DM particle. For splittings of about $\mathcal{O}(1\text{–}10)\%$ of the dark matter mass, this scale ranges from several TeV down to a few hundreds of GeV, which is the prime target space for colored particle searches at LHC [31].

This model exemplifies the approach underpinning the coannihilation codex [23], where the relic density calculation points to the region of parameter space of interest for collider searches. Moreover, this simplified model exhibits a novel dijet resonance + missing transverse energy (MET) signature, which thus far remains an unexplored search channel at the LHC. In contrast to ad hoc models exhibiting this collider signature [32–34], our model readily generates the resonant dijet and MET final state at colliders by recycling vertices used in the coannihilation diagram. Other signals in direct detection and indirect detection experiments are also predicted by reordering the topology of the coannihilation diagram. In this way, we highlight the versatility and power of the coannihilation approach where all features of the DM annihilation mechanism connect to phenomenological signatures at dark matter experiments.

Field	$(\mathrm{SU}(3)_C, \mathrm{SU}(2)_L, \mathrm{U}(1)_Y)$	Spin assignment
DM	(1, 1, 0)	Majorana fermion
X	(3, 1, -2/3)	Dirac fermion
M	(3, 1, -2/3)	Scalar

Table 1. Field content, Standard Model gauge quantum numbers, and spin assignments for the scalar diquark case study ST6. Electric charge is defined as $Q \equiv T_3 + \frac{1}{2}Y$, where T_3 is the third component of weak isospin.

In section 2, we present the field content, Lagrangian, and general phenomenology of our s-channel diquark mediated DM coannihilation model. We show the relic density results for this model in section 3, demonstrating that favorable regions in parameter space are within reach of the LHC. We also briefly comment on the direct detection and indirect detection prospects. In section 4, we review the existing collider bounds for our s-channel diquark mediator and our color triplet coannihilation partner, and also extrapolate these bounds to $100\,\mathrm{fb}^{-1}$ of $13\,\mathrm{TeV}$ LHC luminosity. We study the sensitivity of our proposed dijet resonance + MET collider signature in section 5, highlighting the fact that this novel signature both probes new parameter space outside the reach of current searches as well as makes the DM coannihilation connection manifest. We conclude in section 6.

2 Diquark mediated coannihilation

As emphasized in the coannihilation codex [23], simplified models that explicitly model the dark matter annihilation mechanism offer unique phenomenology previously neglected in dark matter studies. The codex classifies dark matter simplified models by the Standard Model (SM) gauge charges of the dark sector and mediator fields and the s-channel, t-channel, four point, or hybrid (both s-channel and t-channel) topology of the coannihilation diagram. Having such a classification enables a clear and thorough exploration of the signature space of dark matter at colliders, aiding in the prioritization of searches and helping to identify unexplored final states. These experimental signatures are in fact guaranteed in this framework, since they result from stitching together production modes and decay vertices dictated by SM gauge interactions and the coannihilation diagram.

2.1 An s-channel example: the ST6 model

One exemplary model to consider is ST6 ("s-channel mediator, color triplet model 6" from table 4 of reference [23]), which features an s-channel coannihilation topology with a fermionic color triplet coannihilation partner X, scalar color triplet mediator M, and a fermionic SM gauge singlet dark matter DM. The field definitions are shown in table 1. This model is especially attractive to consider because both the coannihilation partner X and the mediator M can be pair-produced at the LHC via strong interactions. The corresponding large pair production rates for these particles could lead to immediate LHC discovery prospects. Moreover, this model juxtaposes signatures reminiscent of supersymmetry with unique collider signatures characteristic of s-channel coannihilation, which highlights the

importance of our bottom-up approach to DM model building. Other s-channel color triplet, sextet, and octet models in the coannihilation codex [23] also share much of the same phenomenology as ST6, and thus the analysis we present is representative of many models detailed in the codex.

Given the field content in table 1, the Lagrangian for this model is

$$\mathcal{L} = \mathcal{L}_{\text{DM}} + \mathcal{L}_{\text{X}} + \mathcal{L}_{\text{M}} + \mathcal{L}_{\text{vis}} + \mathcal{L}_{\text{dark}} \,,$$

$$\mathcal{L}_{\text{DM}} = \frac{i}{2}\overline{\text{DM}}\slashed{\partial}\text{DM} - \frac{m_{\text{DM}}}{2}\overline{\text{DM}}\,\text{DM} \,,$$

$$\mathcal{L}_{\text{X}} = i\overline{\text{X}}\slashed{D}\text{X} - m_{\text{X}}\overline{\text{X}}\,\text{X} \,,$$

$$\mathcal{L}_{\text{M}} = (D_\mu \text{M})^\dagger (D^\mu \text{M}) - m_{\text{M}}^2 \text{M}^* \text{M} - \lambda_{\text{HM}}\left(H^\dagger H\right)\text{M}^*\text{M} - \lambda_{\text{M}}\left(\text{M}^*\text{M}\right)^2 \,,$$

$$\mathcal{L}_{\text{vis}} = -\varepsilon_{abc}\text{M}_a \overline{u_b^C}\left(Y_{ud}^L P_L + Y_{ud}^R P_R\right)d_c - Y_{u\ell}\text{M}_a^*\overline{\ell_R^C}u_R^a - Y_{QL}\text{M}_b^*\left(\overline{L_{L\,\alpha}^C}\varepsilon^{\alpha\beta}(Q_L)_\beta^b\right) + \text{h.c.} \,,$$

$$\mathcal{L}_{\text{dark}} = -y_D\overline{\text{X}}\,\text{DM}\,\text{M} + \text{h.c.} \,, \tag{2.1}$$

where H denotes the SM Higgs field, a, b, and c denote color indices, α and β denote $\text{SU}(2)_L$ weak isospin indices, C is the charge conjugation operator, and we have suppressed flavor indices on Y_{ud}^L, Y_{ud}^R, $Y_{u\ell}$ and Y_{QL}. The Yukawa interactions in $\mathcal{L}_{\text{vis}}$ are written in the mass basis for all quarks and leptons. We need a Cabibbo-Kobayashi-Maskawa (CKM) rotation to write d_L in the mass basis, therefore $Q_L = (u_L, V_{\text{CKM}}d_L)$ for mass eigenstates.[1]

The gauge quantum numbers allow for additional couplings between X or DM and the SM fields. For example, X shares the same quantum numbers as the right-handed down-type quarks, and hence a Yukawa interaction between X, the SM Higgs, and Q_L would lead to mixing between X and the SM down-type quarks after the Higgs acquires a vev. Then, the DM particle would decay to three quarks via a mixing angle insertion, which is phenomenologically ruled out. Separately, DM could have a Yukawa interaction with the Higgs and the left-handed lepton doublet, which would immediately lead to mixing with active neutrinos or other sterile neutrino phenomenology, depending on the mass generation mechanism for SM neutrinos. In order to ensure our DM particle is an appropriate dark matter candidate, we impose a global $\mathbb{Z}_2$ symmetry under which both the DM and X are odd while the mediator and all SM particles are even. Once this $\mathbb{Z}_2$ symmetry is introduced, only the interactions shown in equation (2.1) remain.

The field content in table 1 and Lagrangian in equation (2.1) lead to the s-channel coannihilation diagram depicted in figure 1. We reiterate that the prescription from reference [23] for constructing simplified models is based solely on the coannihilation topology and SM gauge representation assignments. As a result, the parameter space of a given model may have significant constraints coming from flavor physics, proton decay bounds, Higgs physics, and vacuum stability, among others. We discuss these questions in the remainder of this section and will find that interesting and viable parameter space regions are still allowed for model ST6, from which we motivate our LHC study focused on dijet resonances and MET.

---

[1]Note that $\text{SU}(2)_L$ invariance can be made manifest in $\mathcal{L}_{\text{vis}}$ by rewriting the first Lagrangian term as $-Y_{QQ}^{ij}\varepsilon_{abc}M_a\left(\overline{Q_{L\,\alpha}^{C\,b,i}}\varepsilon^{\alpha\beta}(Q_L)_\beta^{c,j}\right) - Y_{ud}^R\varepsilon_{abc}M_a\left(\overline{u_{Rb}^C}d_{Rc}\right)$, and identifying Y_{ud}^L with $2Y_{QQ}V_{\text{CKM}}$.
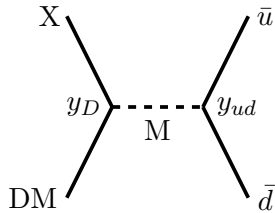
Figure 1. Coannihilation diagram for the model ST6, with a diquark mediator M, coannihilation partner X, and dark matter DM. The Yukawa couplings y_D and y_{ud} denote the mediator couplings to dark sector particles and SM particles, respectively.

2.2 Low energy constraints

In this section, we investigate the constraints on the flavor structure of the Yukawa matrices shown in $\mathcal{L}_{\text{vis}}$ in equation (2.1). First, we note that the simultaneous presence of all Yukawa matrices in $\mathcal{L}_{\text{vis}}$ generates diquark-mediated diagrams that induce proton decay, which is very strongly constrained. For example, if $(Y_{QL})_{11}$ and $(Y_{ud}^L)_{11} = (Y_{ud}^R)_{11} = y_{ud}$ are each nonzero, our mediator generates the decay process $p \to e^+ \pi^0$, which has a minimum lifetime of at least 8.2×10^{33} years [2]. Correspondingly, the product of these couplings is limited to be $\sqrt{y_{ud}(Y_{QL})_{11}} < 4 \times 10^{-17}(m_{\text{M}}/\text{GeV})$. As usual, however, these proton decay bounds can be avoided by extending the accidental baryon and lepton global symmetries of the SM to the new physics particles. If we charge M with baryon number $B = 2/3$ and $L = 0$, for instance, the Y_{QL} and $Y_{u\ell}$ matrices identically vanish. We will hence turn off these couplings, enabling the dijet resonance signature at the LHC instead of the leptoquark resonance, given that the leptoquark case study was presented in reference [23].

Next, we focus on possible flavor-violating entries in Y_{ud}^L and Y_{ud}^R, which are highly constrained by low energy flavor violation probes. Because our mediator has electric charge $-1/3$, it does not induce any tree-level $\Delta F = 2$ meson mixing, which instead occurs via box diagrams. For instance, simultaneous $(Y_{ud}^L)_{11}$ and $(Y_{ud}^L)_{12}$ diquark couplings induce large K^0–$\bar{K}^0$ mixing, leading to the constraint $m_M \gtrsim 10^3 (Y_{ud}^L)_{11}(Y_{ud}^L)_{12}$ TeV [35–37]. Note that the $(Y_{ud}^L)_{11}$ coupling alone also induces K^0–$\bar{K}^0$ mixing via W-boson vertex corrections, but the resulting matrix element is three-loop, doubly-Cabibbo and weak coupling suppressed. If the K^0–$\bar{K}^0$ box diagram involves both chiralities, the experimental constraint is more stringent, requiring $m_M \gtrsim 10^4 (Y_{ud}^{ij})^2$ TeV where i, j are light quark flavor indices. Multiple diagonal entries in Y_{ud}^L are also constrained, since nonzero $(Y_{ud}^L)_{11}$ and $(Y_{ud}^L)_{22}$ couplings also lead to K^0–$\bar{K}^0$ mixing via M and $W^\pm$ mixed box diagrams. The resulting bound requires $m_M \gtrsim 100\sqrt{(Y_{ud}^L)_{11}(Y_{ud}^L)_{22}}$ TeV. Diagonal entries in Y_{ud}^R are much less constrained by this diagram because of a chiral quark mass suppression.

We note that while arbitrary flavor structures in $\mathcal{L}_{\text{vis}}$ are incompatible with proton decay and flavor violation constraints, these flavor aspects are orthogonal to the primary relic density motivation of the model. Thus, for the remainder of the section, in addition to the $B = 2/3$ and $L = 0$ global charges of M, we will set $(Y_{ud}^L)_{11} = (Y_{ud}^R)_{11} = y_{ud}$ and set all other entries of Y_{ud}^L and Y_{ud}^R to zero to satisfy these flavor constraints. This flavor structure, while sufficient for our purposes in discussing the relic density connection

to LHC signatures, is overly restrictive given the constraints above, however, and fuller discussions of possible flavor aspects of scalar diquarks can be found in references [36, 37]. Finally, electroweak oblique corrections can also constrain the X and M masses in our model, but these corrections decouple quickly for X and M masses even moderately above the electroweak scale [38].

2.3 Vacuum stability and precision Higgs physics

We now consider the impact of the Higgs portal quartic coupling λ_{HM} in $\mathcal{L}_M$ for both the stability of the electroweak vacuum and precision Higgs physics. While this term is again irrelevant for the suitability of this coannihilation model regarding relic density, the magnitude of this coupling cannot be constrained by global or gauge symmetries and can have significant phenomenological effects.

First, we note that a large, negative value for λ_{HM} will destabilize the electroweak vacuum and cause the diquark mediator to obtain a vacuum expectation value (vev), which is phenomenologically unacceptable. Hence, we require $m_M^2 + \lambda_{HM} v^2/2 > 0$, where v is the Higgs vev, $H = \frac{1}{\sqrt{2}}(v + h)$. In addition, we impose $\lambda_M > 0$ and $\lambda_{HM} + \sqrt{\lambda_H \lambda_M} > 0$, with λ_H the SM Higgs quartic coupling, to ensure a global vacuum stability [39].

The quartic coupling λ_{HM} is also constrained from Higgs physics, since the mediator M propagates in the loop-induced gluon fusion Higgs production process. In the limit where the top mass and m_M are heavy compared to the Higgs mass, we can calculate the gluon signal strength $\mu_{ggF} \approx \left| 1 + c_M \lambda_{MH} v^2/(8 m_M^2) \right|^2$ [40, 41], where $c_M = 2 \times 4/3$ is proportional to the quadratic Casimir for a color triplet complex scalar. The ATLAS and CMS combination of Higgs measurements constrain $\mu_{ggF} = 1.03^{+0.17}_{-0.15}$ [42], which implies $-0.8 < \lambda_{HM} < 1.2$ for $m_M = 500\,\text{GeV}$. The Higgs decay rate to photons is affected by the charged mediator running in the loop. However, since contributions to this decay mode from intermediate scalars are suppressed by v^2/m_M^2 [43] and the electric charge, the effect of the mediator on the Higgs diphoton decay width will be small even for large λ_{HM}.

As the quartic couplings are not relevant for the collider analysis or relic density calculation, we will simplify the remaining discussion by neglecting the terms λ_{HM} and λ_M. If, however, Higgs data begins to show significant deviations from the SM expectation and a dijet signal emerges from our proposed analysis in section 5, we can revisit the impact of λ_{HM} to both fit the deviations to our model and predict additional signatures given by the coannihilation topology.

2.4 Phenomenological features

As described in the previous sections, the various Yukawa structures and quartic couplings appearing in $\mathcal{L}_{vis}$ and $\mathcal{L}_M$ can lead to unacceptable proton decay, flavor violation, vacuum instability, and Higgs physics effects. We readily satisfy all of these bounds, however, by giving baryon number 2/3 and lepton number 0 to M, restricting $(Y_{ud}^L)_{11} = (Y_{ud}^R)_{11} = y_{ud}$ as the only nonzero entries in Y_{ud}^L and Y_{ud}^R, and neglecting the quartic scalar couplings in $\mathcal{L}_M$.

These simplifications lead to a small number of physical parameters in our simplified model: the masses of the mediator, X, and DM, the visible coupling y_{ud}, and the dark coupling y_D. We define $\Delta \equiv (m_X - m_{DM})/m_{DM}$ to be the fractional mass splitting between

the coannihilation partner X and the dark matter, and we always assume X is heavier than DM, which ensures the stability of the DM particle. Since DM is a SM gauge singlet, it is only produced at the LHC in the decays of X or M, where both X and M can be pair-produced from SM gauge interactions. We also can singly-produce M via the coupling y_{ud}, giving a dijet resonance or the very difficult M $\to (jj)_{\text{soft}} + \not{E}_T$ channel.

The coannihilation partner X has only a single decay mode, X $\to$ DM $\bar{u}\bar{d}$, which is prompt as long as Δ is not extremely small. Pair production of X then leads to the $2(jj)_{\text{soft}} + \not{E}_T$ final state, where the softness of the outgoing jets is correlated with Δ. If Δ is small, these soft jets will escape detection and the primary signature will be $\not{E}_T$ accompanied with one or two jets from initial/final state radiation. This signature is already probed by the ATLAS and CMS monojet searches [17, 20] and by the lowest multiplicity signal regions of the multijet + MET searches [44–47]. For large Δ and large DM mass, the jets from the X decay can be hard enough to pass detector thresholds, leading to signatures akin to gluino pair production in the minimal supersymmetric standard model (MSSM) [8, 44]. Moreover, because DM is a SM gauge singlet, Δ plays a dominant role in determining the DM relic density via the X–X and X–DM annihilation modes in the effective DM annihilation cross section [24].

The diquark mediator can either decay via the visible coupling y_{ud} or the dark sector coupling y_D. The corresponding partial widths, assuming massless quarks, are

$$\Gamma\left(\text{M} \to \bar{u}\bar{d}\right) = \frac{y_{ud}^2}{4\pi} m_{\text{M}} \,,$$
$$\Gamma\left(\text{M} \to \text{X DM}\right) = \frac{y_D^2}{8\pi} m_{\text{M}} K(\Delta, \tau_{\text{DM}}) \,, \tag{2.2}$$

where, for on-shell M $\to$ X DM decays, $\tau_{\text{DM}} \equiv m_{\text{DM}}^2/m_{\text{M}}^2$ and

$$K(\Delta, \tau_{\text{DM}}) \equiv \left(1 - \Delta^2 \tau_{\text{DM}}\right)^{\frac{1}{2}} \left(1 - (2 + \Delta)^2 \tau_{\text{DM}}\right)^{\frac{3}{2}} \,. \tag{2.3}$$

The possible final states for M pair production are $2(jj)_{\text{res}}$, $(jj)_{\text{res}} + (jj)_{\text{soft}} + \not{E}_T$, and $2(jj)_{\text{soft}} + \not{E}_T$, where we denote the decay products from X as soft because of the fractional mass splitting Δ. While the pair production of dijet resonances has been a traditional new physics signature, the mixed decay $(jj)_{\text{res}} + (jj)_{\text{soft}} + \not{E}_T$ gives a striking dijet resonance + MET final state which remains unexplored. Section 5 will present a proposed analysis and the experimental prospects for this interesting mixed decay signature.

The relative rates between the three M M* final states are dictated by the visible branching fraction B,

$$B \equiv \text{Br}\left(\text{M} \to \bar{u}\bar{d}\right) = \frac{y_{ud}^2}{y_{ud}^2 + \frac{1}{2}y_D^2 K(\Delta, \tau_{\text{DM}})} = \frac{B_0}{B_0 + (1 - B_0)K(\Delta, \tau_{\text{DM}})} \,,$$
$$B_0 \equiv \text{Br}\left(\text{M} \to \bar{u}\bar{d}\right)\big|_{m_{\text{DM,X}}=0} = \frac{y_{ud}^2}{y_{ud}^2 + \frac{1}{2}y_D^2} \,, \tag{2.4}$$

where we introduce B_0 to represent the mediator M branching fraction into SM particles at zero dark matter mass and coannihilation partner mass. We note that the couplings y_{ud}

and y_D can be traded for B_0 or B and the total width of M, which are natural variables to discuss the collider constraints and prospects on M. Hence, we adopt the language of m_{DM}, Δ, m_M, B_0 or B, and Γ_M to tighten the connection between the relic density calculation and collider probes.

We implement the diquark triplet model in `FeynRules v2.3.18` [48, 49] with the Lagrangian in equation (2.1) using the simplifications summarized in the beginning of this subsection. This implementation is publicly available in the FeynRules model database [50], where an interface with Monte Carlo generators is also available using the `UFO` [51] format. Our relic density calculations in section 3 are performed using `MicrOMEGAs v4.1.8` [52] through `CalcHEP v3.6.25` [53] output of `FeynRules`. We also performed cross-checks of our relic density calculation using `MadDM v2.0` [54, 55]. The collider recasting discussion in section 4 and the mixed decay study shown in section 5 use simulated Monte Carlo events generated from `MadGraph5 v1.5.14` [56, 57]. We shower and hadronize the events using `Pythia v8.2` [58] and perform detector simulation with `Delphes v3.2` [59] using the default CMS parameter card. When indicated, matching between the hard matrix element and the parton shower is performed using the MLM matching scheme [60].

3 Relic density

The central concern for the simplified models developed in the coannihilation codex [23] is the dark matter relic density. By modeling the dark matter annihilation mechanism, we can directly connect the parameter space of a given simplified model to phenomenological signals in direct detection experiments, indirect detection experiments, and colliders. Hence, the relic density calculation features strongly in motivating our discussion of experimental signatures, and we can demonstrate the particular interplay between different terrestrial and astrophysical probes manifest in our diquark mediator case study.

In this vein, we calculate the parameter space that gives the correct dark matter relic density, $\Omega h^2 = 0.1198 \pm 0.0026$ [1, 2] for the ST6 model, subject to the Lagrangian flavor restrictions discussed in section 2. The three fields, DM, X, and M, and two couplings, y_{ud} and y_D, lead to several channels that determine the final DM relic density. Since the dark matter candidate is a pure SM gauge singlet fermion, the usual pair annihilation channel $\overline{DM}\,DM \to \overline{SM}\,SM$ vanishes at tree level and can be neglected. Obtaining the appropriate relic density for DM therefore depends crucially on X and M. In particular, DM and X readily stay in thermal equilibrium with SM particles until thermal freeze out from Hubble expansion in the early universe, where the process that freezes out last determines the relic density [24].

There are four categories of two-to-two (co)annihilation channels relevant for the diquark model:

DM X $\to$ SM$_1$ SM$_2$: the standard coannihilation channel where DM and X coannihilate to SM particles $\bar{u}\bar{d}$ through the s-channel diquark mediator. This channel is dominant only when the diagram is resonant, that is when $m_{DM} + m_X \sim m_M$.

$\overline{\mathrm{X}}$ X $\to$ $\overline{\mathrm{SM}}$ SM: pair annihilation of X into SM pairs. Since X is a color triplet, pair annihilation of X into gluons and quarks is typically dominant, especially for low X masses when other channels are kinematically closed. As long as DM and X are in chemical equilibrium, this channel sets a lower bound on m_{DM} for a given value of Δ: ever lighter DM and X masses cause Ωh^2 to fall below the measured DM relic density and hence underclose the universe.

DM X $\to$ M V_{SM}: real radiation of a SM gauge boson ($V_{\mathrm{SM}} = g, \gamma, Z$) from the on-shell production of M. This category of channels opens up whenever $m_{\mathrm{DM}} + m_{\mathrm{X}} \gtrsim m_{\mathrm{M}}$ and is generated whenever X or M radiates off a SM gauge boson. Since X and M are colored, this category is dominated by the gluon radiation diagram.

$\overline{\mathrm{DM}}$ DM $\to$ M* M: DM pair annihilation to a pair of mediators. The last channel only opens up when $m_{\mathrm{DM}} \gtrsim m_{\mathrm{M}}$. This pair annihilation mode of DM is generated through a t-channel X exchange and gives the only contribution to the effective coannihilation cross section which is not exponentially suppressed by Δ. The $\overline{\mathrm{X}}$ X $\to$ M* M process also exists but is subdominant to X pair annihilation to SM particles.

We note that the Sommerfeld effect modifies the cross section for the process $\overline{\mathrm{X}}$ X $\to \bar{q}q$, gg, where the t-channel exchange of soft gluons can potentially lead to significant non-perturbative effects. We use the calculation of the Sommerfeld enhancement factors for colored particles in reference [11] and implement this in `MicrOMEGAs` [61]. In contrast to the results of reference [11], however, we find that the Sommerfeld enhancement effects are less than a few percent on the relic density for the parameters we consider because of a cancellation between the enhancement of the cross section in the channel $\overline{\mathrm{X}}$ X $\to gg$ and the suppression in the channel $\overline{\mathrm{X}}$ X $\to \bar{q}q$. We therefore neglect this effect in our relic density calculations.

In figure 2, we plot the dark matter relic density as a function of the DM mass for various choices of mediator mass, Δ, and Yukawa couplings $y_{ud} = y_D = y$. We also overlay the measured relic density with 3σ uncertainties from Planck [1] as a gray horizontal band. In the bottom panel, the relative contributions from the four different annihilation categories are displayed for a single benchmark point. This breakdown of the overall relic density calculation into constituent annihilation and coannihilation channels reinforces the importance of explicitly accounting for all fields and diagrams that contribute to the dark matter relic density.

3.1 Relic density favored regions

We now use the relic density calculation to motivate masses and couplings to probe with collider experiments, while direct detection and indirect detection prospects are discussed in section 3.2. From figure 2, we see that perturbative Yukawa couplings for TeV-scale mediators and electroweak scale dark sector particles generally give the correct DM relic density. As a result, because M and X can be pair produced via strong interactions at the LHC, we expect a dynamic interplay between the parameter space region favored by the relic density calculation, the current exclusion bounds from ATLAS and CMS, and the
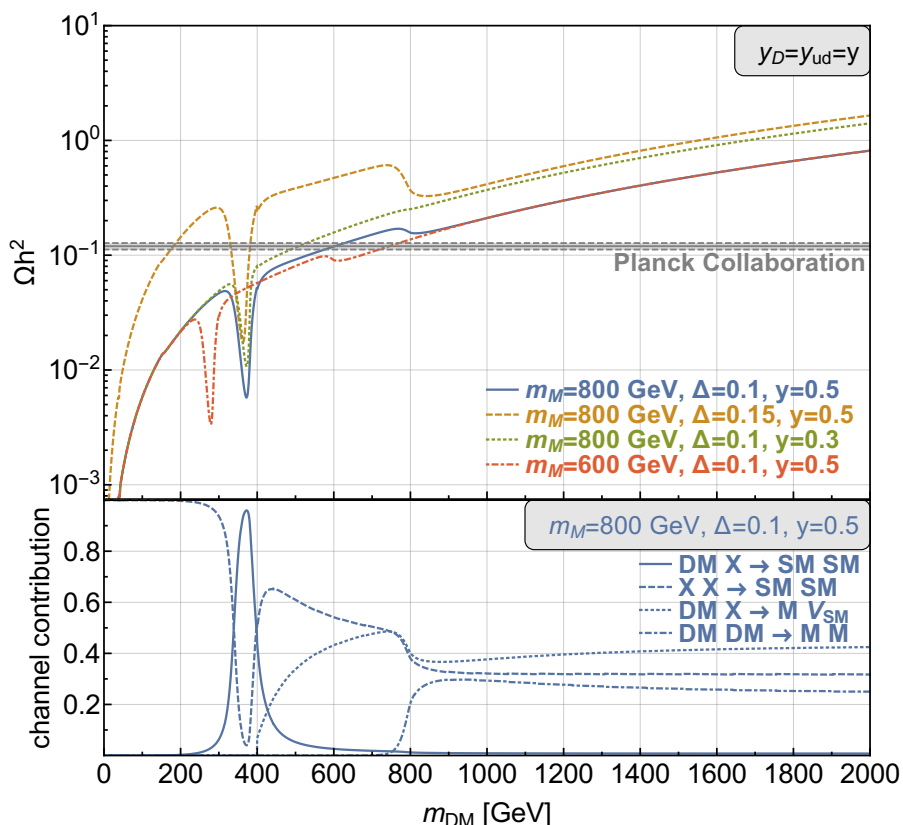
Figure 2. Upper panel: the relic density in the triplet diquark model ST6 as a function of the dark matter mass for given values of $m_{\rm M}$, fractional mass splitting Δ, and $y_{ud} = y_D = y$, where the gray horizontal band shows the Planck measurement with 3σ uncertainty [1]. Lower panel: the relative contributions from the four different channels described in the text are shown for a single benchmark point.

discovery prospects from future searches. Following section 2, we adopt $m_{\rm DM}$, Δ, $m_{\rm M}$, B_0 and $\Gamma_{\rm M}$ as the five parameters of our model. Recall B_0 from equation (2.4) is the particular coupling relation defining the zero mass visible branching fraction of the diquark mediator, and $\Gamma_{\rm M} = \Gamma\left({\rm M} \to \bar{u}\bar{d}\right) + \Gamma\left({\rm M} \to {\rm DM}X\right)$ from equation (2.2) is the total mediator width.

In figure 3, we scan the $m_{\rm DM}$ vs. $m_{\rm M}$ plane for $B_0 = 0.1$ and $\Delta = 0.125$, where $B_0 = 0.1$ is equivalent to requiring $y_D^2 = 18 y_{ud}^2$. We overlay regions with $\Gamma_{\rm M}/m_{\rm M} \leq 10^{-1}$, 10^{-2}, 10^{-3}, and 10^{-4}, which effectively scan over y_{ud} and y_D given the proportionality above. We see that heavy DM masses, which generally overclose the universe as depicted from the asymptotic behavior in figure 2, still recover the correct Ωh^2 if the DM X $\to$ SM$_1$ SM$_2$, DM X $\to$ M $V_{\rm SM}$, and $\overline{\rm DM}$ DM $\to$ M* M channels are large enough. If the width of the mediator is small, however, the DM X $\to$ M $V_{\rm SM}$ and $\overline{\rm DM}$ DM $\to$ M* M channels become negligible. Then, the correct relic density is only found in the resonant coannihilation region, or when the everpresent $\overline{\rm X}$ X $\to$ $\overline{\rm SM}$ SM channel together with the given Δ produce the appropriate effective DM annihilation cross section to fall into the measured band of Ωh^2. The upper and lower lobes for $\Gamma_{\rm M}/m_{\rm M} \leq 10^{-3}$ show the separate impact of the $\overline{\rm DM}$ DM $\to$ M* M and DM X $\to$ M $V_{\rm SM}$ channels, respectively, avoiding
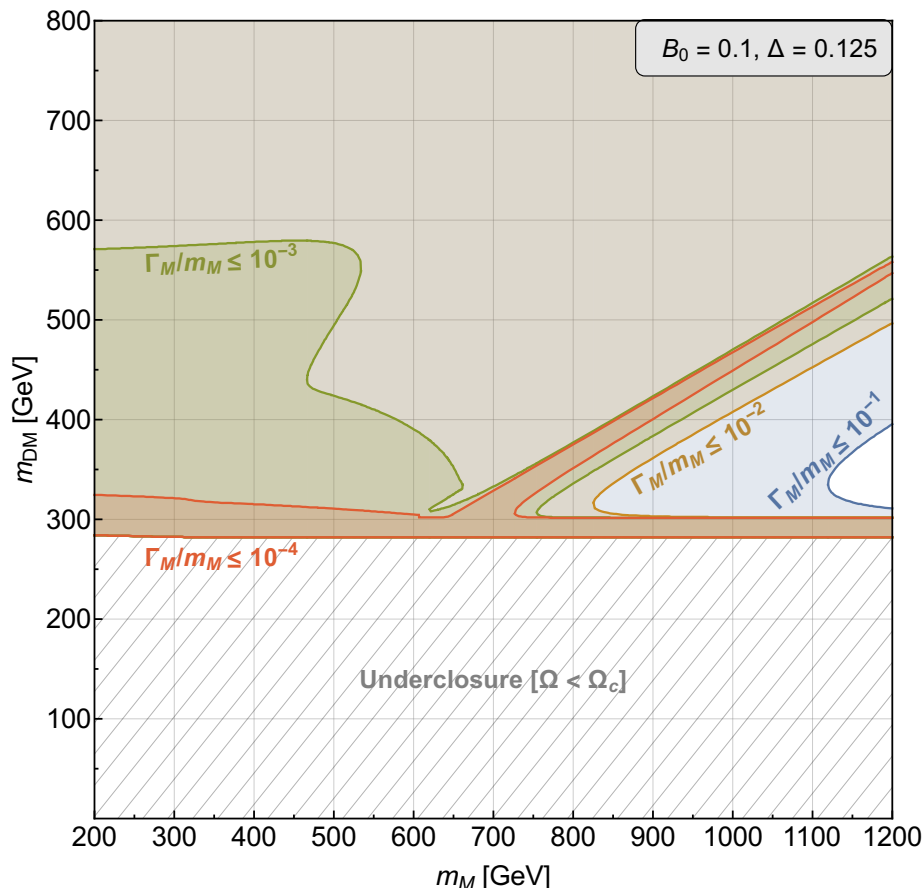
Figure 3. Parameter space consistent with the measured relic density within 3σ from Planck [1], for fixed $B_0 = 0.1$ and $\Delta = 0.125$ in the $m_{\rm DM}$ versus $m_{\rm M}$ plane, with different overlays of maximal $\Gamma_{\rm M}/m_{\rm M}$.

overclosure of the universe by supplementing the $\overline{\rm X}\,{\rm X} \to \overline{\rm SM}\,{\rm SM}$ channel. Because our model always includes the $\overline{\rm X}\,{\rm X} \to \overline{\rm SM}\,{\rm SM}$ channel, and because we always assume a sufficient y_D coupling to keep DM and X in chemical equilibrium [23], we underclose the universe for $\mathcal{O}(100\,{\rm GeV})$ DM masses for $\Delta = 0.125$, regardless of B_0. For these light DM masses, the SM gauge interactions ensure that the $\overline{\rm X}\,{\rm X} \to \overline{\rm SM}\,{\rm SM}$ process rapidly depletes the DM relic density. To have a viable DM model in this underclosure region, we would either have to increase Δ, which expressly suppresses the $\overline{\rm X}\,{\rm X} \to \overline{\rm SM}\,{\rm SM}$ contribution to the effective DM annihilation cross section, or we would require additional field content outside of our simplified model.

This interesting dependence on Δ is shown in figure 4, where we have chosen $B_0 = 0.1$ and scanned the Yukawa couplings such that $\Gamma_{\rm M}/m_{\rm M} \leq 10^{-4}$. Most strikingly, we see that the choice of Δ sensitively changes the boundary between underclosure and overclosure delineated by the $\overline{\rm X}\,{\rm X} \to \overline{\rm SM}\,{\rm SM}$ process, shown in the horizontal shaded bands. The diagonal bands aligned with $m_{\rm DM} + m_{\rm X} \sim m_{\rm M}$ correspond to the resonant coannihilation process. We see that the horizontal bands become wider for larger $m_{\rm DM}$, and this growth is larger on the left side of the coannihilation funnel compared to the right side. The overall
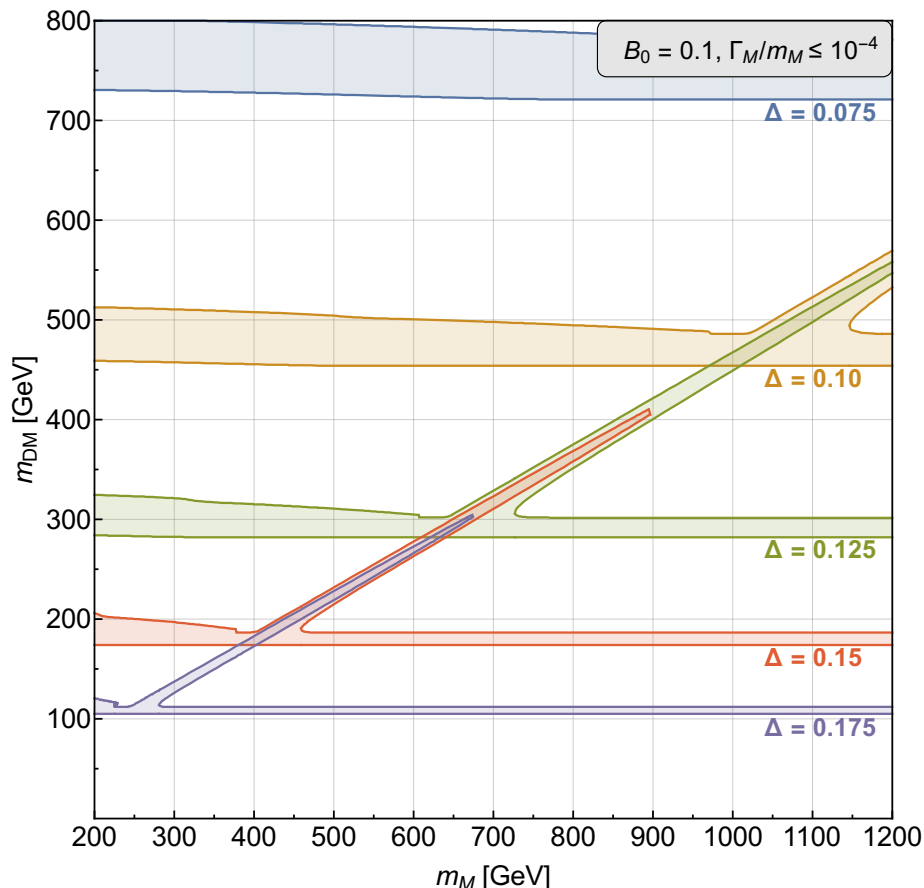
Figure 4. Parameter space consistent with the measured relic density within 3σ from Planck [1], for fixed $B_0 = 0.1$ and scanning over $\Gamma_{\rm M}/m_{\rm M} \leq 10^{-4}$, with different choices of Δ overlaid.

width of the bands is determined by the relative flattening of the relic density curve as $m_{\rm DM}$ increases, as evident in figure 2. On the left side of the coannihilation funnel, however, the opening of the DM X $\rightarrow$ M $V_{\rm SM}$ and $\overline{\rm DM}$ DM $\rightarrow$ M* M channels enhance the effective annihilation cross section and avoid DM overclosure of the universe.

We see from figure 4 that the choice of Δ effectively sets the dark matter mass scale at which the correct relic abundance is achieved. On the other hand, $m_{\rm DM}$ and Δ directly set the energy scale of the X decay products in the X $\rightarrow \bar{u}\bar{d}$ DM decay and hence control the complementarity between searches for X pair production and probes for the diquark mediator. Intriguingly, the combination of $m_{\rm DM}$ from 300 GeV to 500 GeV and $\Delta \sim 0.1$ results in a spectrum of X decay products that straddles the jet thresholds used in current multijets and MET searches [44]. Therefore, we present a detailed discussion of the current collider bounds for signatures of both X and M in section 4.

Finally, we briefly comment on generalizing these conclusions to the entire set of codex models with a strongly interacting coannihilation partner X and a SM gauge singlet DM. Given X and DM are in chemical equilibrium, the $\overline{\rm X}$ X $\rightarrow$ $\overline{\rm SM}$ SM annihilation channel will always dominate for low DM masses and hence connect the choice of Δ to a particular relic density motivated energy scale for $m_{\rm DM}$, leading to the behavior seen in figure 4. In general,

larger QCD representations for X will increase the efficacy of this coannihilation channel, driving the relic density motivated scale of $m_{\rm DM}$ even lower for a given Δ. Moreover, the different X and DM representations will change the relative importance of the non-perturbative Sommerfeld effect [11, 61]. A full quantitative description of relic density constraints for dark matter models with a strongly interacting coannihilation partner will be the subject of a future work.

3.2 Direct and indirect detection prospects

We now address the direct detection prospects for the ST6 s-channel diquark mediator DM model. For $\Delta \sim 0.1$ and X and DM masses in the few hundred GeV range, the coannihilation partner X decays promptly and will have vanishing relic density today. Since DM has no SM gauge quantum numbers, all of the DM direct detection interactions are loop-induced and scale at least with the new physics coupling y_D. These loop-induced diagrams, though, are not inherently responsible for determining the dark matter relic density and thus the relic density requirement will not have a meaningful bearing on the direct detection prospects.

Since the momentum transfer in DM-nucleon scattering is $\mathcal{O}(100\text{ MeV})$, and our DM mass scale is at least $100\,\mathrm{GeV}$, we can use an effective field theory description based on the Lagrangian in equation (2.1) and integrating out M, X, and the high momentum modes of DM to analyze the leading DM direct detection prospects. We find three loop-induced operators that can drive DM direct detection:

$\overline{\mathbf{DM}}$ **DM** $H^\dagger H$**:** this is the leading dimension-five operator, which is loop-induced by X and M internal legs and requires a nonzero Higgs portal coupling $\lambda_{\rm HM}$. This operator scales as $(y_D^2 \lambda_{\rm HM})/(16\pi^2 m_{\rm M})$ and effects DM direct detection once the Higgs acquires a vev. Since the quartic coupling $\lambda_{\rm HM}$ is arbitrary, however, the impact of this operator for direct detection can be completely negligible.

$\overline{\mathbf{DM}}$ **DM** $\bar{u}u$**,** $\overline{\mathbf{DM}}$ **DM** $\bar{d}d$**:** these dimension-six operators arise from insertions of X, M and quark fields and can be written schematically as $\left[\overline{\rm DM}\,\Gamma^{\rm DM}\,{\rm DM}\right] \times [\bar{q}\,\Gamma^q\,q]$, where $\Gamma^{\rm DM}$ and Γ^q enumerate the possible Lorentz-invariant contractions (see, e.g. references [4, 6]). Because the DM is a Majorana particle, however, the pure vector $\Gamma^{\rm DM} = \gamma^\mu$ and tensor $\Gamma^{\rm DM} = \sigma^{\mu\nu}$ contractions vanish. The axial vector current $\Gamma^{\rm DM} = \gamma^\mu\gamma^5$ is also absent, because the hypercharge couplings of X and M induce purely vector Z and photon currents after electroweak symmetry breaking. The remaining possibilities are scalar bilinears, which require a chiral flip in the quark sector and are thus suppressed by $m_q/m_{\rm M}^3$, which is too small to be constrained by direct detection.

$\overline{\mathbf{DM}}$ **DM** $G^a_{\mu\nu} G^{a,\mu\nu}$**:** this dimension-seven operator is induced by X and M internal legs. After integrating out the internal legs, this operator scales with $(\alpha_s y_D^2)/(4\pi m_{\rm M}^3)$, and the strong suppression by the loop factor and three powers of m_M implies we can safely ignore its contribution to the DM direct detection cross section. Similarly, the dimension-seven operator with $B_{\mu\nu}B^{\mu\nu}$ instead of $G^a_{\mu\nu}G^{a,\mu\nu}$ is further suppressed by α'/α_s.

In summary, the direct detection interactions in our model are all driven by higher dimensional operators, and if λ_{HM} is small, none of these operators are expected to give a meaningful direct detection DM-nucleon cross section.

Regarding indirect detection signals, we can have loop-induced pair annihilation of DM using the operators listed above. The first operator results in final state Higgs bosons or any pair of SM gauge bosons or matter particles, while the second and third operators give final state quarks and gluons, and the aforementioned $\overline{\mathrm{DM}}$ DM $B_{\mu\nu}B^{\mu\nu}$ dimension-seven operator gives photons and Z bosons. If $m_{\mathrm{DM}} < m_{\mathrm{M}}$, then DM can annihilate to $ud\bar{u}\bar{d}$ via one or two off-shell diquark mediators, but this process is phase-space suppressed compared to the dimension-six scalar bilinear operator. The operator scaling behavior from the direct detection discussion also applies for the indirect detection signals, given the lack of resonant enhancement in these processes. If $m_{\mathrm{DM}} > m_{\mathrm{M}}$, we have the pair annihilation of DM into $\mathrm{M}^* \mathrm{M}$, which then decay to quarks. Because DM is a Majorana fermion, however, this annihilation channel is p-wave suppressed. Therefore, the indirect detection signals from this model are dim.

4   Existing searches

In this section, we discuss the existing collider constraints on our triplet diquark model. The visible mediator decays are constrained by searches for single and pair-produced dijet resonances, while the coannihilation partner X and the DM are probed via monojet searches as well as multijets + MET searches. These collider signatures arise from stitching together gauge interactions of M and X with the interaction vertices inherent in the coannihilation diagram in figure 1.

Following the discussion in section 2.4, we recast the searches for single dijet resonances, pair-produced dijet resonances, monojets, and MSSM gluinos to constrain the masses and couplings of our diquark mediator, coannihilation partner, and the DM. A striking signature absent in current searches by ATLAS and CMS, however, is the promising mixed decay channel from pair-produced mediators, which we present in section 5.

4.1   Single and paired dijet resonance searches

Dijet resonance searches set bounds on the mediator mass and couplings in this model. Our relic density results in figures 3 and 4 point to mediator masses of $200\,\mathrm{GeV}$ to $1200\,\mathrm{GeV}$ as especially attractive to target via dijet resonance searches. Furthermore, since our diquark mediator is a color triplet, single dijet searches and paired dijet searches probe complementary sets of new physics couplings.

Many dijet resonance searches constrain the $pp \to \mathrm{M} \to \bar{u}\bar{d}$ channel (for an overview, see reference [62], and see reference [63] regarding the DM context). The latest $8\,\mathrm{TeV}$ search from CMS [64] uses data scouting to constrain dijet resonances as light as $500\,\mathrm{GeV}$, and the $8\,\mathrm{TeV}$ ATLAS search [65] uses pre-scaled jet triggers to obtain limits on resonances as light as $250\,\mathrm{GeV}$. The ud diquark nature of our mediator dictates stronger single resonance constraints from pp colliders instead of $p\bar{p}$ colliders like Sp$\bar{\mathrm{p}}$S and Tevatron, hence we do not present the UA2 [66], CDF Run 1 [67], or CDF Run 2 [68] constraints.

In the CMS scouting analysis, events are required to have $H_T > 250\,\text{GeV}$, where H_T is the scalar p_T sum of jets with $p_T > 30\,\text{GeV}$ and $|\eta| < 2.5$ and jets are clustered using the anti-k_T algorithm with distance parameter $R = 0.5$. The leading and subleading jets in p_T are used as seeds to form wide jets, which add together jets closer than $R = 1.1$ to the nearer seed jet. The wide jets must have $\Delta\eta < 1.3$ to reduce QCD background and an invariant mass larger than $390\,\text{GeV}$ to ensure a smoothly falling spectrum. The ATLAS search clusters jets with the anti-k_T algorithm and $R = 0.6$, and events must have two jets with $p_T > 50\,\text{GeV}$ and rapidity $|y| < 2.8$. These jets must have a rapidity separation $\Delta y < 1.2$ and an invariant mass $m_{jj} > 250\,\text{GeV}$.

Given a narrow mediator M, with $\Gamma_{\text{M}}/m_{\text{M}} \lesssim 10^{-1}$, the single dijet production rate scales as $\sigma(y_0, m_{\text{M}})(y_{ud}^2/y_0^2)B$, where $\sigma(y_0, m_{\text{M}})$ is the cross section calculated using a reference visible coupling y_0 and mediator mass m_{M} and B is the visible branching fraction as defined in equation (2.4). For diquarks decaying purely to dijets, $B = 100\%$ and the bound on the coupling is extracted by equating $\sigma(y_0, m_{\text{M}})(y_{ud,\text{excl}}^2/y_0^2) = \sigma_{\text{excl}}$ for an excluded cross section σ_{excl} from experiment. When the X DM decay is kinematically accessible, though, it is more convenient to constrain the visible branching fraction B for fixed choices of the total width Γ_{M}, since these parameters encode the entire dependence of the signal dijet rate. The excluded visible branching fraction is determined by equating $\sigma(y_0, m_{\text{M}})(y_{ud}^2/y_0^2)B_{\text{excl}} = \sigma(y_0, m_{\text{M}})B_{\text{excl}}^2\Gamma_{\text{M}}/\Gamma_0 = \sigma_{\text{excl}}$, where $\Gamma_0 = y_0^2\text{M}/(4\pi)$ is the visible width determined by the reference coupling y_0. These exclusions from CMS [64] and ATLAS [65] are shown in figure 5 for $\Gamma_{\text{M}}/m_{\text{M}} = 3 \times 10^{-4}$, 5×10^{-4}, and 10^{-3}. We see that larger total mediator widths lead to stronger exclusions, since the overall dijet resonance rate increases with the total mediator width. Nevertheless, single dijet constraints are not sensitive to total widths smaller than $\Gamma_{\text{M}}/m_{\text{M}} = 10^{-4}$, hence we use $\Gamma_{\text{M}}/m_{\text{M}} = 10^{-4}$ as an upper limit on the total mediator width in our calculations in section 5.

Pair-produced diquarks are dominantly produced via color interactions, and the corresponding paired dijet signal scales with B^2 if the dark decay M $\to$ X DM is kinematically open. For $m_{\text{M}} < m_{\text{DM}} + m_{\text{X}}$, though, the dark decay is closed and paired dijet searches probe mediator masses independently of the visible coupling y_{ud}. The single and paired dijet searches are otherwise complementary, given that the single dijet mass reach is typically higher than the paired dijet mass reach.

There are paired dijet searches by CMS using $7\,\text{TeV}$ [69] and $8\,\text{TeV}$ [70] data. Each dijet pair must fulfill requirements on ΔR_{jj} and then the combination of the two pairs that minimizes $\Delta m/m_{\text{avg}}$ is selected. To suppress the QCD continuum background, a further cut on the p_T imbalance versus the average mass of the dijet pairs is imposed, ensuring a smoothly falling distribution in the average mass. This distribution is used to obtain cross section limits on a pair-produced dijet resonance with masses between $200\,\text{GeV}$ and $1000\,\text{GeV}$ for the $8\,\text{TeV}$ search, which supersedes the old result. There is also an ATLAS $7\,\text{TeV}$ analysis [71], but this covers the mass window ranging from $150\,\text{GeV}$ to $350\,\text{GeV}$ and is less constraining than the $8\,\text{TeV}$ search by CMS.

Hence, we use the most constraining $8\,\text{TeV}$ CMS analysis [70], which gives the cross section limit as $\sigma \times B^2$. We recast their limit using `NLL-fast v2.1` [72–75] in combination with `CTEQ v6.6` [76] parton distribution functions (PDFs) to calculate m_{M} dependent next-
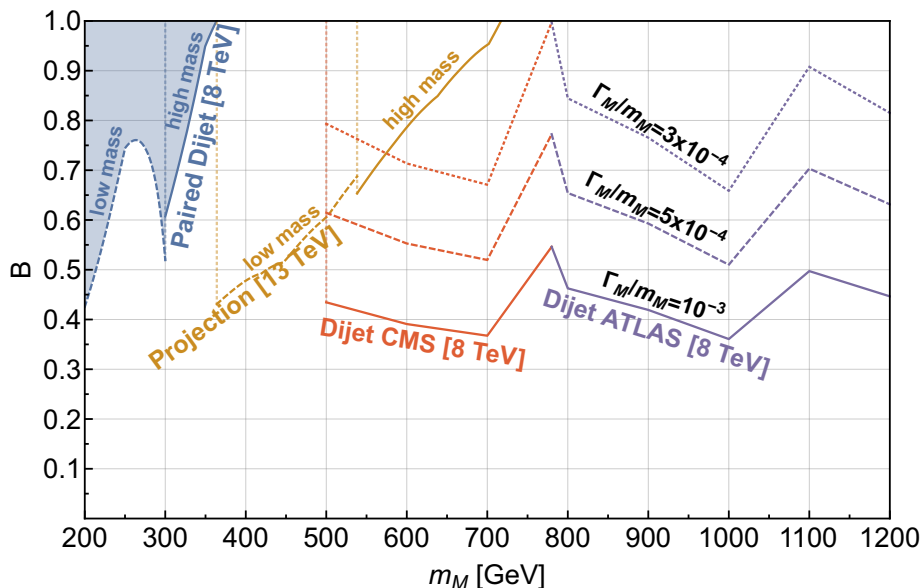
Figure 5. The existing limits from searches for paired dijet resonances are shown, where the CMS search (blue line) [70] is most constraining. The orange line shows the projected exclusion by the same search at 13 TeV and 100 fb^{-1} of integrated luminosity. We also show the envelope of dijet resonance searches by CMS (red) [64] and ATLAS (purple) [65] as exclusion contours for different choices of $\Gamma_M/m_M = 3 \times 10^{-4}$ (dotted), 5×10^{-4} (dashed), and 10^{-3} (solid). Only the most constraining dijet resonance search is displayed for a given mediator mass.

to-leading order (NLO) cross sections at 8 TeV LHC. The resulting limits are shown in figure 5 as the shaded blue region, where we have delineated the disjoint low mass and high mass search regions. We see that even low mass mediators are unconstrained by the data if the visible branching fraction is less than 40%.

Using `Collider Reach` [77], we estimate the 13 TeV sensitivity for pair produced dijet resonance searches, assuming an integrated luminosity of 100 fb^{-1}. A similar projection for the dijet resonance limits is not given because these would only alter the maximum value for Γ_M/m_M, and because the mass sensitivity using data scouting techniques by CMS or prescaled jet triggers by ATLAS has not been demonstrated at 13 TeV. Both the low mass and high mass paired dijet search regions are scaled upward, although this is an oversimplification of the potential search strategy at 13 TeV LHC. We expect these rough limits are nonetheless indicative of the possible sensitivity, given that `Collider Reach` simply uses PDF scalings to mimic the production of on-shell resonances when the background and signal are generated by the same partonic scattering channel. The projection is shown as an orange contour in figure 5, where again, visible branching fractions below 40% are not expected to be constrained.

4.2 Jets + MET searches

In contrast to the resonance signatures from our diquark mediator, the coannihilation partner X decays to soft jets and missing transverse energy with a 100% branching fraction.

Search	$\Delta = 0.1$	$\Delta = 0.125$	$\Delta = 0.15$
8 TeV	384 GeV	396 GeV	392 GeV
13 TeV	398 GeV	399 GeV	396 GeV
13 TeV, 100 fb^{-1} projection	464 GeV	468 GeV	477 GeV

Table 2. The 95% C.L. exclusion limits on $m_{\rm X}$ from 8 TeV and 13 TeV jets + MET searches by ATLAS [44, 46] at the LHC, as well the projected exclusion reach for 100 fb^{-1} of 13 TeV luminosity.

Pair production of X can then be constrained by monojet searches as well as multijet + MET searches. The resolved nature of the soft jets depends on the fractional mass splitting Δ and the X mass, which influences the tradeoff in signal sensitivity between the monojet and multijet + MET searches. Jets from initial state radiation (ISR), however, skew the search sensitivity to the multijet + MET searches, especially for light X masses.

Since X is a color triplet fermion, we can calculate the pair production cross section for X using `Top++ v2.0` [78] interfaced with `LHAPDF v6.1` [79] and the `NNPDF v3.0` [80] set to obtain NLO signal cross sections for arbitrary X masses. Using `CheckMate v1.2` [81], we find the 8 TeV jets + $\not{E}_T$ search by ATLAS [44] imposes the strongest constraints on the X mass for various choices of Δ. This search considers a wide range of signal regions characterized by the number of hard jets observed in the event and the value of the effective mass $m_{\rm eff}$, defined as the scalar p_T sum of all jets with $p_T > 40$ GeV plus the $\not{E}_T$. The most powerful region for our signal is the "2-jet medium" region, that, in particular, requires $m_{\rm eff} > 1.2$ TeV in addition of two hard jets. Since Δ is typically small, the two hard jets observed for our signature come from ISR. The relatively relaxed event selection implies this search region is systematics limited, where ATLAS quotes a 6.6% systematic uncertainty for a background expectation of 760 events. The related "2-jet tight" and "4-jet loose" regions, with $m_{\rm eff}$ cuts of 1.6 and 1.0 TeV, respectively, are also sensitive to our final state but are less powerful than the "2-jet medium" region and have larger systematic uncertainties of about 8%. We remark that although the strongest bounds for this search are obtained by tagging on ISR jets, the traditional ATLAS monojet search [20] leads to much weaker bounds for our choices of Δ. On the other hand, we expect that dedicated analyses beyond the monojet and multijet + MET searches can improve the sensitivity to compressed spectra [82, 83].

We show the 95% confidence level (C.L.) exclusion limits on the X mass for $\Delta = 0.1$, 0.125, and 0.15 in table 2. Note we neglect the impact of the mediator pair production here, which can give the same final state via the M* M $\rightarrow 2(jj)_{\rm soft} \not{E}_T$ decay chain. Since this decay is only kinematically open once $m_{\rm M} \geq m_{\rm X} + m_{\rm DM}$, this process pays the suppression factors of a much smaller pair production cross section of M and the dark decay branching fraction $(1 - B)^2$ compared to the X pair production rate. Our results rule out X masses below about 390 GeV for the $\Delta \sim 0.1$ values motivated by figure 4.

The ATLAS and CMS collaborations have both updated their jets + MET searches at 13 TeV [45, 46], which are not included in the `CheckMate` catalogue yet. Given the slightly

larger luminosity of ATLAS, we recast the ATLAS search only and expect the CMS bounds to be similar. Using the Monte Carlo pipeline described in the end of section 2.4, we cross check our MLM matched sample of signal events with the cut flow efficiencies of the signal regions described in reference [46]. We use our derived signal acceptance fractions to compute 95% C.L. exclusions on m_X. Our model is most constrained by the "2-jet loose" and "2-jet medium" signal regions of reference [46], which require at least two hard jets + MET as well as a loose or medium cut on the effective mass. Our limits on m_X are shown in the middle row of table 2, showing a minor improvement over the 8 TeV results.

In order to compare with the projected sensitivity of our mixed mediator search described in section 5, we extrapolate the jets + MET search to $100 \, \text{fb}^{-1}$ of integrated luminosity. Assuming the current systematic uncertainties are unchanged, we rescale the background and signal events by the luminosity ratio for the 2-jet loose signal region to obtain a projected 95% C.L. exclusion on the X mass. Since the 2-jet loose and 2-jet medium signal regions are already dominated by systematic uncertainties, the increase in integrated luminosity does not significantly improve the bounds on the visible cross section and thereby on m_X. Our results are in the last row of table 2, which show that X masses of about 470 GeV are expected to be probed in future multijet + MET searches.

4.3 Summary of conventional searches

To summarize, we have studied the existing constraints and future sensitivity from the conventional LHC searches. We first discussed the dijet resonance searches targeting single and pair production of the mediator, where the bounds are collected in figure 5. The single production bounds constrain $B \lesssim 35\%$ for $\Gamma_M/m_M = 10^{-3}$, although this bound is completely absent once $\Gamma_M/m_M = 10^{-4}$. Current pair production limits constrain mediators below 360 GeV for B varying between about 45% and 100%, though this bound is strongest only for mediators near 200 GeV. The projected reach of the paired dijet search with $100 \, \text{fb}^{-1}$ of 13 TeV data covers mediator masses between 360 GeV to 720 GeV, but this relies on a simple extrapolation of the low mass and high mass reach from 8 TeV. We conclude that mediators heavier than 360 GeV with $\Gamma_M/m_M \leq 10^{-4}$ are unconstrained by the current single and paired dijet searches, which leaves a large, open parameter space to explore with future dijet searches and our proposed mixed decay search described in section 5.

We then discussed the multijet + MET searches, which target X pair production and the $X \rightarrow (jj)_{\text{soft}} \not{E}_T$ decay. Our resulting limits on the X mass, shown in table 2, have a mild dependence on Δ, since Δ sets the hardness of the jets from the X decay. The jets + MET searches, however, are already dominated by systematic uncertainties, and so they are not expected to improve dramatically with $100 \, \text{fb}^{-1}$ of 13 TeV data. Our recasting and projection of the ATLAS 13 TeV search [46] shows an improvement on the m_X limit from 400 GeV to 460 GeV. The results should be juxtaposed with figure 3, where the $\Delta = 0.125$ to $\Delta = 0.10$ relic density regions straddle the current and expected exclusion limits from the jets + MET search. This coincidence in the relic density motivated region indicates that the LHC has excellent prospects for discovering a colored coannihilation mechanism akin to our s-channel diquark model, and it also emphasizes the importance of the overlooked dijet resonance + MET channel, which we discuss next.
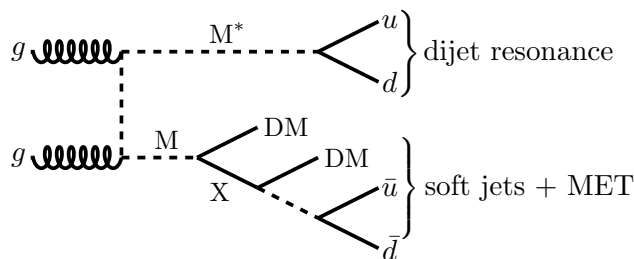
Figure 6. An example process for the mixed decay signature from pair produced mediators. One mediator decays visibly to a dijet resonance, and the other decays to DM and X, giving soft jets and missing transverse energy.

5 Mixed decay phenomenology

As highlighted in section 2.4, pair production of our diquark mediator can lead to the unique signature of a dijet resonance accompanied by missing transverse energy. The resonance + MET final state was also previously emphasized as a general prediction of coannihilation models with an s-channel mediator [23]. The resonance + MET signature is also particularly motivated because this channel directly tests the coannihilation diagram from figure 1. Since the rate for this signature is sensitive to the ratio of the dark and visible new physics couplings via the mediator branching fractions, combining results from the mixed and the dijet resonance searches would be central to determining the underlying dark matter Lagrangian. Moreover, the dijet resonance + MET signature together with the relic density calculations presented in section 3 and the single dijet, paired dijets, and jets + MET signatures discussed in section 4 unify into a compelling picture of a bottom-up discovery of dark matter at the LHC. This synthesis will be presented in section 5.4.

The mixed decay of pair-produced mediators leads to a final state of $(jj)_{\rm res} + (jj)_{\rm soft} + \rlap{/}{E}_T$, as shown in figure 6. The typical momenta of the soft jets is determined by the mass splitting between X and DM. As described in section 3, and in most of the parameter space favored by relic density requirements, these momenta are close to the various jet p_T thresholds used by ATLAS and CMS. The primary goal of our analysis is to identify the dijet resonance and large MET signature, while the possible discrimination of additional soft signal jets from X decay will be a minor secondary consideration.

5.1 Event generation

Signal events are generated using the procedure and tools described in section 2. Following the relic density favored regions in figure 4, we focus on $\Delta = 0.1$, 0.125, and 0.15. Given the jets + MET recasting performed in section 4.2, with results summarized in table 2, we know that X is already excluded to about $400 \, {\rm GeV}$ for these choices of Δ, and hence we focus our study on mediators in the several hundred GeV to TeV mass range.

Our new physics signal is characterized by a strong dijet resonance recoiling against large MET. While the intrinsic width of our mediator is constrained to be small by dijet resonance searches, as discussed in section 4.1, we expect the resolution on our narrow

resonance to be dominated by jet energy scale uncertainty as well as jet clustering contamination from ISR, final state radiation (FSR), and the X decay products. For our mediator mass range and choices of Δ, we find these effects are not significant enough to warrant a complex jet substructure analysis to sharpen the dijet peak structure, and we instead ameliorate these effects by optimizing the jet clustering algorithm and clustering radius. Our events are clustered using the anti-k_T algorithm [84] with $R = 0.5$.

Given the final state of a dijet resonance and MET, we study the following backgrounds:

- $(Z \to \nu\nu) + 1, 2$ jets: this background is similar to the final state that we are considering but will typically have a lower $\not{E}_T$ and no resonant structure.

- $(W^\pm \to \ell^\pm\nu) + 1, 2$ jets: this background can be significantly reduced by a lepton veto. If the lepton is not reconstructed, though, the associated signature is similar to the $(Z \to \nu\nu) +$ jets background.

- QCD multijets: while this background has no intrinsic MET, QCD can easily produce fake MET if a jet is badly reconstructed or mismeasured. This $\not{E}_T$ distribution follows a different slope than the vector boson + jets backgrounds above and should lead to a smooth continuum in the dijet invariant mass spectrum.

We do not simulate other backgrounds, which are expected to be subdominant to those listed above. In particular, $t\bar{t}$+jets will be readily reduced by vetoing heavy flavor jets, while the remaining semi-leptonic and fully leptonic $t\bar{t}$ events will only contribute if the leptons are lost, which renders it subdominant to the $W^\pm +$ jets background. Similarly, diboson production where one boson decays invisibly or leptonically and the other hadronically will be a small correction to the $Z +$ jets or $W^\pm +$ jets backgrounds, respectively. To properly model the associated jet distributions for each background, we use MLM matching [60] to avoid double-counting jets from the hard matrix element and jets from the parton shower. The Z and $W^\pm$ backgrounds are matched up to two jets and the QCD multijet background is matched up to three jets, each using a matching scale of 20 GeV.

In order for the Monte Carlo generation to efficiently populate the tails of the background distributions, we sample the phase space following the procedure described in reference [85]. We modify `MadGraph` to implement an S_T^* cut at generator level, where S_T^* is the scalar p_T sum of all generator level particles. We partition the MC generation in S_T^* bins, which follow

$$\sigma_i = \sigma(\texttt{stmin}_i < S_T^* < \texttt{stmax}_i) \gtrsim 0.9 \times \sigma(\texttt{stmin}_i < S_T^*), \tag{5.1}$$

where σ_i is the cross section in the i-th bin and $\texttt{stmax}_i$, $\texttt{stmin}_i$ are the bin edges. The final overflow bin must satisfy $N > 10 \times \sigma_{\text{overflow}} \times L$, where N is the total number of events to be generated in the bin and L is the desired integrated luminosity.

We use `NLL-fast v3.1` [72–75, 86] in combination with `NNPDF v3.0` [80] to calculate m_M dependent NLO-cross sections for pair-production of the mediator at 13 TeV. For our mediator mass range, the K-factor is relatively flat, varying between 1.58 and 1.65 for m_M from 500 to 1500 GeV. The background K-factors are obtained from `MCFM v6.8` [87]

for processes involving electroweak gauge bosons and from references [88, 89] for QCD multijets. The background K-factors are found to be 1.15 for the vector boson backgrounds and 1.3 for QCD multijets.

We apply mild preselection cuts on both the signal and backgrounds, requiring events to have at least two jets, $\not{E}_T > 100\,\text{GeV}$ and the leading jet p_T greater than $80\,\text{GeV}$. These cuts only increase the efficiency of our Monte Carlo event generation and will be superseded by the analysis level cuts. Signal samples are generated with m_{M} starting at $500\,\text{GeV}$, which is the lowest mass our simulation can confidently probe a dijet resonance, and m_{DM} starting at $25\,\text{GeV}$.[2]

5.2 The mixed decay search strategy

As outlined in 5.1, our search strategy targets a signal exhibiting a large amount of $\not{E}_T$, at least two hard jets with a resonant structure, and possible additional resolved jets from X decays, ISR, and FSR. Our main discriminants between signal and background will be MET and the resonant dijet peak over a continuum dijet background. We will also employ angular cuts to improve the overall signal to background ratio in the dijet invariant mass spectrum.

Our cut flow table is shown in table 3. In the first row, we show the $13\,\text{TeV}$ cross sections for each process after applying preselection cuts and K-factors. For comparison, we also show a signal benchmark point with $(m_{\text{DM}}, m_{\text{X}}, m_{\text{M}}) = (379, 417, 900)\,\text{GeV}$. Sequential cuts and cumulative acceptance efficiencies are shown in subsequent rows.

We first apply a lepton veto, which mainly reduces the leptonic $W^{\pm}+$ jets background by about 30%. This low suppression rate is due to the tight lepton isolation requirements of the CMS Delphes card (summed p_T of tracks within a cone of $R = 0.5$ must be less than 10% of the lepton p_T). We expect a veto on leptons using medium or loose identification criteria would improve the $W^{\pm}+$ jets rejection and negligibly impact our signal acceptance. Next, since our diquark mediator is coupled only to first generation quarks, we apply a b-jet veto, which is expected to significantly suppress the subdominant $t\bar{t}$ background. We use the b-tagging efficiencies quoted in reference [90], with a maximum tagging efficiency of 85% and a mistag rate of 0.2%.

We require at least two hard jets, where hard jets have $p_T > 100\,\text{GeV}$ and $|\eta| < 2.5$. This hard jet requirement suppresses the remaining vector boson plus jets backgrounds by about 85% and the QCD background by about 68% while retaining more than 95% of the extant signal. We also cut on events with $\not{E}_T$ arising primarily from jet mismeasurement by requiring $\Delta\phi(j_i, \not{E}_T) > 0.2$ for all hard jets j_i. As expected, this cut significantly reduces QCD, by about a factor of four. We model jet mismeasurements using the default parameters from the CMS card of `Delphes-3.2.0`. Note that, as mentioned in [23], this modeling leads to an overestimate of the tail of the QCD $\not{E}_T$ distribution. Our results can therefore be considered conservative.

Finally, we require the rapidity difference between the two leading hard jets to be less than 1.3, which mimics the cut used in the dijet resonance searches and reflects the

---

[2]`Pythia 8` is not able to correctly process the X decay for the tiny mass splittings associated with lighter DM masses, but in principle, our search strategy will still be sensitive to this region of parameter space.

	signal	$Z_{\nu\nu}$ + jets	$W^+_{\ell\nu}$ + jets	$W^-_{\ell\nu}$ + jets	QCD
σ_{NLO} (pb)	7.60×10^{-3}	93.21	157.33	75.48	6948.76
ℓ veto	100	100	71.4	69.0	100
b-jet veto	86.9	89.3	66.8	64.5	87.3
$p_T(j_1)$, $p_T(j_2)>100\,\mathrm{GeV}$	83.0	11.8	9.76	9.68	27.6
$\Delta\phi(j_i,\not{E}_T)>0.2$	75.0	10.9	8.50	7.99	6.20
$|\Delta\eta(j_1,j_2)|<1.3$	51.5	6.36	5.01	4.82	3.61
$\not{E}_T>900\,\mathrm{GeV}$	6.29 (48)	3.51×10^{-3} (327)	7.74×10^{-4} (122)	2.83×10^{-4} (21)	1.71×10^{-5} (119)
Mass window	3.56 (27)	3.35×10^{-4} (31)	8.70×10^{-5} (14)	1.93×10^{-5} (2)	1.28×10^{-6} (9)

Table 3. Detailed cut flow for a signal benchmark with $(m_{\mathrm{DM}}, m_{\mathrm{X}}, m_{\mathrm{M}}) = (379, 417, 900)\,\mathrm{GeV}$ and the Z + jets, $W^\pm$ + jets, and QCD multijet backgrounds. The cross sections quoted include the preliminary cuts described in section 5.1 and K-factors for 13 TeV LHC. The $\not{E}_T$ and $m_{j_1j_2}$ cuts are optimized for each signal point individually, and we quote both the efficiency (in %) and the number of events at $100\,\mathrm{fb}^{-1}$ luminosity for each process. The dijet mass window considered for this benchmark point is $[812, 987]\,\mathrm{GeV}$.

kinematic configuration expected from figure 6. After these general cuts, the cumulative acceptances for the different backgrounds are of the order of 5%. We obtain our final sensitivity estimates after simultaneously optimizing the $\not{E}_T$ and $m_{j_1j_2}$ mass window cuts for each signal benchmark.

In the left panel of figure 7, we show the stacked $\not{E}_T$ distribution after cuts for the different backgrounds, and overlay our signal benchmark as a black outline. Cutting on $\not{E}_T$ significantly removes the backgrounds, where the rejection factors range from 10^3 for $Z+$ jets to 10^5 for QCD, while the benchmark signal is reduced by less than an order of magnitude, giving a signal to background ratio of $\mathcal{O}(10\%)$. The optimal $\not{E}_T$ cut is correlated with the mediator mass. Furthermore, for low DM masses, jets from the X decay might be boosted enough to pass the detection threshold, thus the amount of $\not{E}_T$ in signal events is also expected to mildly decrease with the DM mass. Note that, at this point of the search, our analysis strategy is similar to the one used in the existing multijet + MET searches, but the resonant structure of the mediator provides a significant handle to dramatically improve the mediator mass reach.

In the right panel of figure 7, we show the $m_{j_1j_2}$ distributions for the signal and the backgrounds after a $\not{E}_T > 900\,\mathrm{GeV}$ cut. Since the background jets do not come from resonances, the background dijet mass spectrum falls smoothly. The signal, however, exhibits a wide peak around the mass of the mediator particle and can be easily identified on top of the backgrounds. To impose an appropriate mass window for the dijet mass spectrum, we fit the signal $m_{j_1j_2}$ distribution after cuts by a Crystal Ball function [91],

$$s(x) = N \times \begin{cases} \exp\left[-\frac{(x-\bar{x})^2}{2\sigma^2}\right] & \text{if } \frac{x-\bar{x}}{\sigma} > -\alpha, \\ \left(\frac{n}{|\alpha|}\right)^n \exp\left(-\frac{|\alpha|^2}{2}\right)\left(\frac{n}{|\alpha|} - |\alpha| - \frac{x-\bar{x}}{\sigma}\right)^{-n} & \text{if } \frac{x-\bar{x}}{\sigma} \le -\alpha. \end{cases} \tag{5.2}$$

Here N is the normalization, $\bar{x}$ and σ are Gaussian parameters, and α and n are power law parameters, all determined by the fit. We integrate the number of events within 2σ of the
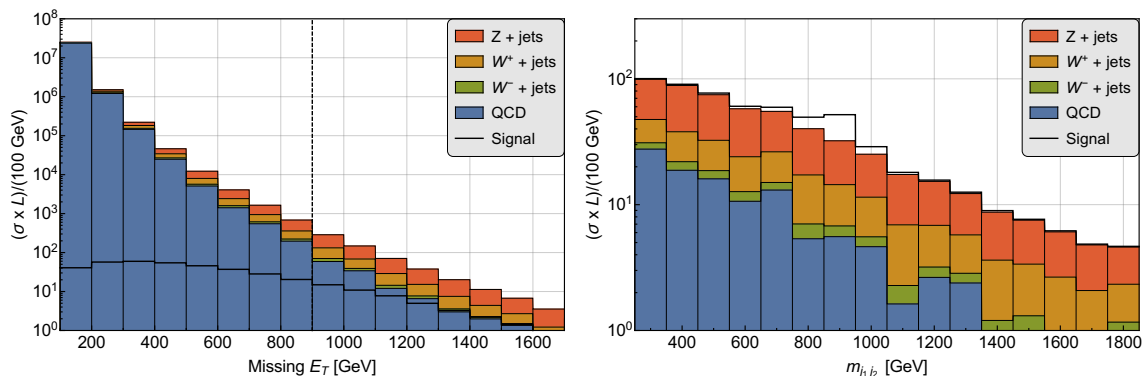
Figure 7. Signal and background $\not{E}_T$ (left) and $m_{j_1 j_2}$ (right) distributions for a signal benchmark model with $(m_{\mathrm{DM}}, m_{\mathrm{X}}, m_{\mathrm{M}}) = (379, 417, 900)\,\mathrm{GeV}$. The signal distribution is shown in black outline. The stacked background distributions are from top to bottom: $Z+$ jets (red), $W^+ +$ jets (orange), $W^- +$ jets (green) and QCD (blue). The vertical dashed line at $900\,\mathrm{GeV}$ on the left panel represents the optimal $\not{E}_T$ cut for this benchmark point. The $m_{j_1 j_2}$ distribution is shown for events that passed this $\not{E}_T$ cut.

Gaussian mean, $\bar{x}$, for the signal and the background samples to calculate the significance,

$$\mathcal{S} = \frac{S}{\sqrt{\sum B_i + (\sum \mathrm{sys}_i \times B_i)^2}}, \tag{5.3}$$

where sys_i is the systematic uncertainty for a given background B_i, and S and B_i are the number of signal and background events in the mass window, respectively. Following reference [46], we take $\mathrm{sys}_i = 5\%$ for the W and Z backgrounds, while we use 20% for the QCD multijet background, because of the lack of simulated events in the tail of the $\not{E}_T$ distribution.

We optimize the $\not{E}_T$ cut by maximizing the dijet resonance significance $\mathcal{S}$. The last two rows of table 3 show the efficiencies as well as expected number of events for $100\,\mathrm{fb}^{-1}$ of $13\,\mathrm{TeV}$ LHC data given the benchmark-specific $\not{E}_T > 900\,\mathrm{GeV}$ cut and the dijet mass window cut, $812\,\mathrm{GeV} \le m_{j_1 j_2} \le 987\,\mathrm{GeV}$.

In order to estimate robustly the number of background events in the mass window after the $\not{E}_T$ cut without being limited by Monte Carlo statistics, we fit each background $m_{j_1 j_2}$ distribution by a falling function of the form [65]

$$b(x) = p_0 (1-x)^{p_1} x^{p_2 + p_3 \ln x}, \tag{5.4}$$

where $x = m_{j_1 j_2}/\sqrt{s}$. For each background, we then integrate $b(x)$ with the optimal p_i parameters over the chosen mass window to obtain the number of background events after the $m_{j_1 j_2}$ cuts.

5.3 Sensitivity of the mixed decay search

The results of our collider study for $\Delta = 0.125$ are shown in figure 8 for $100\,\mathrm{fb}^{-1}$ of $13\,\mathrm{TeV}$ luminosity. We illustrate the mixed sensitivity with three contours corresponding
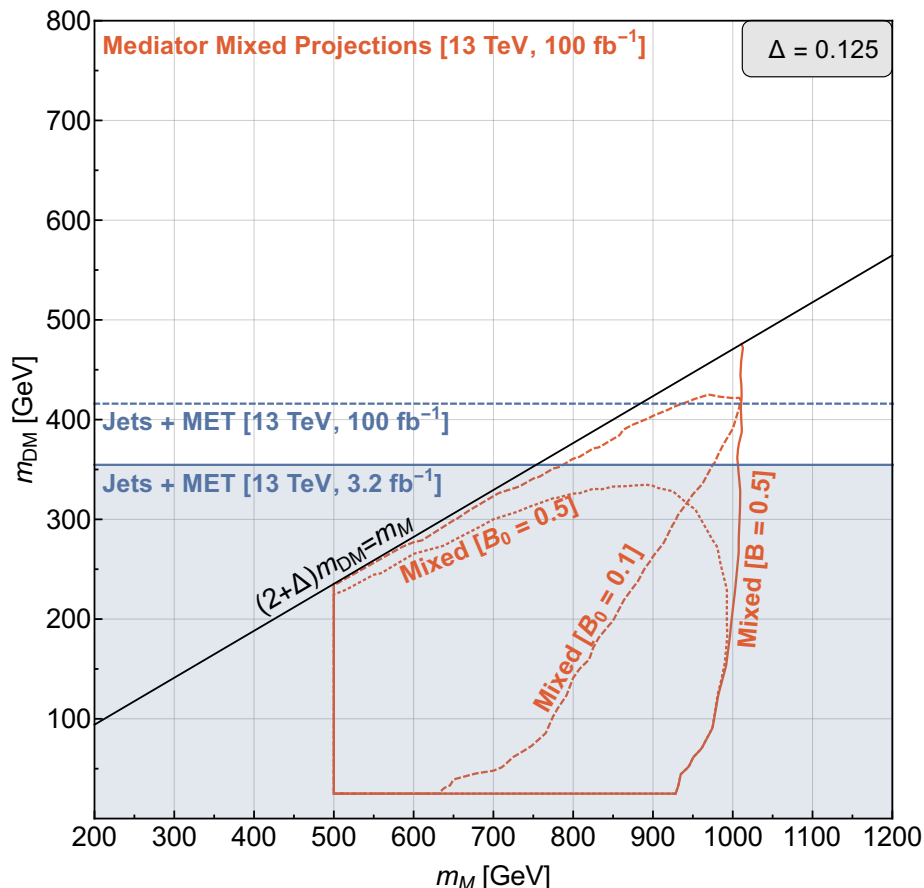
Figure 8. Comparison in LHC sensitivity between the existing jets + MET searches and the newly proposed mixed topology in the DM mass vs. mediator mass plane with $\Delta = 0.125$. The mixed search sensitivity is shown for $B_0 = 0.1$, $B_0 = 0.5$, and $B = \mathrm{Br}\left(\mathrm{M} \to \bar{u}d\right) = 0.5$ as an ideal scenario. For given values of m_{DM} and m_{M}, this ideal rate can always be ensured by choosing B_0 accordingly.

to $B_0 = 0.1$, $B_0 = 0.5$, and $B = 0.5$. Recall that fixing B_0 is equivalent to fixing a particular coupling combination of y_{ud} and y_D via equation (2.4), while the physical branching fraction of the mediator to dijets depends on B_0 and the phase space of the $\mathrm{M} \to \mathrm{X}$ DM decay. Alternately, fixing B requires the couplings to change as a function of the M and DM masses. In particular, as we move along the $B = 0.5$ contour in figure 8, B_0 is monotonically decreasing to zero up to the phase space boundary of $(2 + \Delta)m_{\mathrm{DM}} = m_{\mathrm{M}}$.

As expected, by changing from $B_0 = 0.5$ to $B_0 = 0.1$, the expected reach of the dijet resonance + MET search moves closer to the phase space boundary of $(2+\Delta)m_{\mathrm{DM}} = m_{\mathrm{M}}$. The $B_0 = 0.5$ reach is coincident with the $B = 0.5$ reach for low DM masses since the phase space suppression of $K(\Delta, \tau_{\mathrm{DM}})$ is negligible. By construction, the intersection point between the $B_0 = 0.1$ and $B = 0.5$ contours indicates when the phase space suppression factor maximizes the overall rate for the mixed decay signature from M pair production, $\sigma(pp \to \mathrm{M}^*\mathrm{M}) \times 2B(1-B) \xrightarrow[B=0.5]{} 0.5 \times \sigma(pp \to \mathrm{M}^*\mathrm{M})$. The $B = 0.5$ choice also fixes the paired dijet resonance rate to $0.25 \times \sigma(pp \to \mathrm{M}^*\mathrm{M})$ when the $\mathrm{M} \to \mathrm{X}$ DM decay is on-

shell. The $B_0 = 0.1$ and $B = 0.5$ contours indicate that a significant portion of parameter space in the $m_{\rm DM}, m_{\rm M}$ plane will be tested by the mixed decay search from section 5.2. This search is also complementary to the current and future reach from the jets + MET searches for X pair production, indicated by the shaded and horizontal lines at $m_{\rm DM} \sim 360\,{\rm GeV}$ and $m_{\rm DM} \sim 420\,{\rm GeV}$ in figure 8, respectively. These two searches test integral processes predicted by the coannihilation mechanism, and the simultaneous observation of both channels would be a striking sign of s-channel coannihilation at the LHC.

5.4 Connecting the relic density to collider searches

As emphasized in reference [23] and throughout this paper, our simplified models based on modeling the DM annihilation mechanism allow us to develop collider searches that target the parameter space favored by the measured Ωh^2. Moreover, for our model, direct detection and indrect detection signals are suppressed compared to the collider probes, and thus the relic density parameter space will mainly be confronted by the existing LHC searches discussed in section 4 and our proposed mixed decay analysis from section 5.2. This bottom-up approach directly connects the relic density requirement to the LHC signature space, enforcing the role of LHC as a DM producing machine.

As discussed in section 3, DM (co)annihilation to SM particles occurs through numerous subprocesses with different dependencies in the new physics couplings y_{ud} and y_D. These couplings, though, are significantly constrained by the dijet resonance searches described in section 4.1. As a result, in the parameter space region where DM has the correct relic density and satisfies the dijet constraints, the relic density will be driven by $\overline{\rm X}\,{\rm X}$ annihilation via strong interactions or DM X resonant coannihilation. This was illustrated in figure 4, where the chosen $B_0 = 0.1$ parameter and $\Gamma_{\rm M}/m_{\rm M} \leq 10^{-4}$ scan led to Ωh^2 favored regions for each value of Δ. The relic density analysis points to $\Delta \sim 10\%$ for DM and mediator masses within reach of the LHC, although the exact preferred region depends sensitively on Δ, as shown in figure 4.

The prospects of different LHC searches as well as the region allowed by relic density constraints are shown in figure 9 for $0.10 \leq \Delta \leq 0.125$. For this Δ range, the correct relic density is obtained for dark matter masses between 300 to 500 GeV or in the funnel region. Following the discussion in section 3.1, the relic density region constricts to a horizontal band driven by $\overline{\rm X}\,{\rm X} \to \overline{\rm SM}\,{\rm SM}$ and a coannihilation funnel parallel to the $(2 + \Delta)m_{\rm DM} = m_{\rm M}$ line. Furthermore, $\Delta = 0.125$ corresponds to the lower edge of the horizontal band, while $\Delta = 0.1$ corresponds to the upper edge.

While $m_{\rm DM} \lesssim 360\,{\rm GeV}$ is excluded by the recasted 13 TeV jets + MET search by ATLAS discussed in section 4.2, the projected limit of this search with $100\,{\rm fb}^{-1}$ luminosity is only expected to improve to $m_{\rm DM} \sim 425\,{\rm GeV}$ and will only cover part of the favored relic density region. Similarly, the relic density region is excluded for $m_{\rm M} \lesssim 360\,{\rm GeV}$ by the 8 TeV search for paired dijet resonances, but this search weakens dramatically below the kinematic threshold $(2 + \Delta)m_{\rm DM} = m_{\rm M}$ because of the rapid turn-on of the M $\to$ X DM decay for our choice of $B_0 = 0.1$. Nevertheless, the $100\,{\rm fb}^{-1}$ projection for paired dijet searches should reach mediator masses of about 720 GeV, giving an independent test of
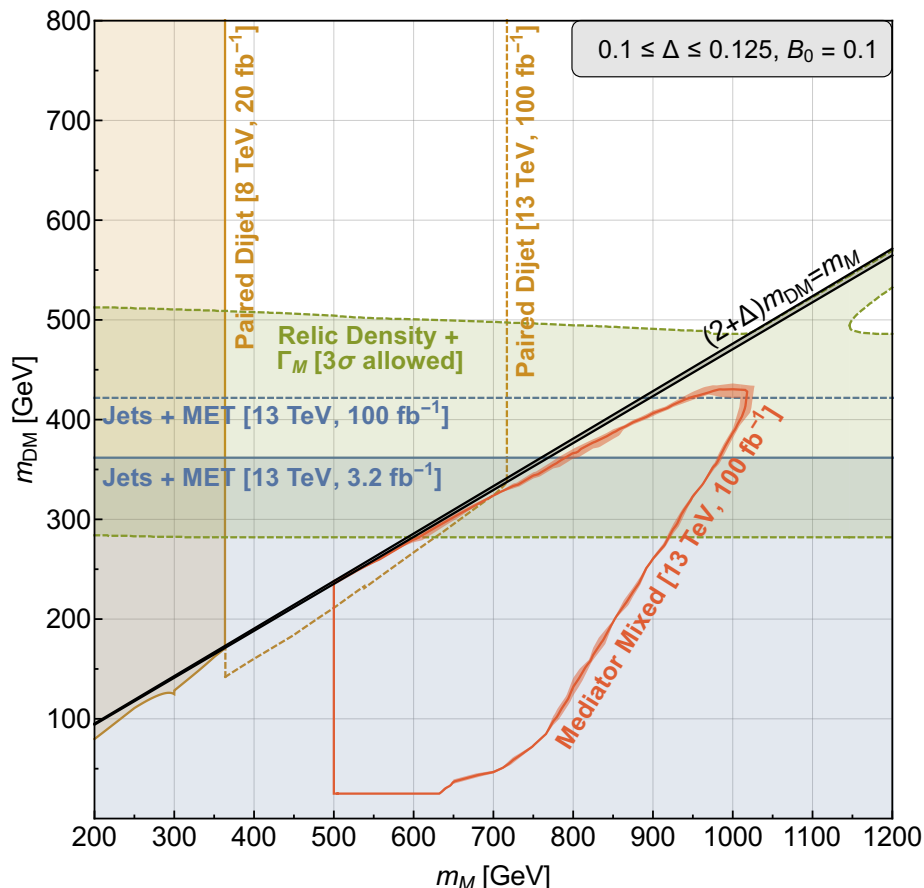
Figure 9. Summary plot for $0.1 \leq \Delta \leq 0.125$ and $B_0 = 0.1$ in the dark matter mass versus mediator mass plane. The relic density region is determined by scanning over mediator couplings requiring $\Gamma_M/m_M \leq 10^{-4}$ and matching the Planck measurement of Ωh^2, allowing a 3σ deviation from the central value. The current $13\,\text{TeV}$, $3.2\,\text{fb}^{-1}$ limit from recasting the ATLAS jets + MET search [46] and the projection with $100\,\text{fb}^{-1}$ luminosity are shown in solid and dashed blue lines, adopting the strongest limit according to the variation in Δ. The current $8\,\text{TeV}$, $20\,\text{fb}^{-1}$ and future $13\,\text{TeV}$, $100\,\text{fb}^{-1}$ paired dijet limits are shown as mostly vertical orange contours. Our proposed search for the novel signature of a dijet resonance + MET is shown for $100\,\text{fb}^{-1}$ of $13\,\text{TeV}$ data as a red contour with shading to indicate the dependence on Δ. The black diagonal lines span the kinematic threshold $(2 + \Delta)m_{\text{DM}} = m_{\text{M}}$ for on-shell decays of the mediator to X DM.

the relic density region above the $(2 + \Delta)m_{\text{DM}} = m_{\text{M}}$ line compared to the $100\,\text{fb}^{-1}$ jets + MET projection.

Moreover, for on-shell decays of the mediator to X DM, the new mediator mixed decay search introduced in sections 5.2 and 5.3 probes an orthogonal decay mode to the paired dijet search and also complements and enhances the jets + MET reach. We remark that fixing $B = 0.5$ gave a uniform reach for the mediator mixed search at about $m_{\text{M}} = 1\,\text{TeV}$, as shown in figure 8, and so the mixed decay search clearly has parameter space sensitivity beyond that expected from the jets + MET projection. In the fortunate case of excesses in both the mixed decay search and the jets + MET search, an immediate goal would be

to test whether the mediator is consistent with an *s*-channel coannihilation mechanism. Multiple, well-motivated searches covering complementary signatures of the same relic density region is a hallmark feature of simplified models in our coannihilation framework, since these signatures result from recycling vertices and gauge number assignments inherent in the DM coannihilation diagram.

6   Conclusions

The enigmatic dark matter question remains at the forefront of particle physics research today. Discovering the particle properties of dark matter would represent a pinnacle achievement in the fields of particle physics and astrophysics. Hence it is crucially important to identify all viable dark matter search strategies for present and future experiments.

Building on the general classification of simplified coannihilating dark matter models [23], we studied the relic density predictions, indirect and direct detection constraints, and collider phenomenology of a dark matter particle coannihilating with a strongly interacting partner. We adopted model ST6 from reference [23] as a case study, where the DM is an electroweak singlet Majorana fermion, the coannihilation partner X is a color triplet fermion, and the *s*-channel mediator M is a scalar color triplet. Besides the three masses, the only other relevant parameters in this simplified model are the y_D coupling between the mediator, X, and DM, and the y_{ud} coupling between the mediator and the SM up and down quarks, ensuring consistency with flavor constraints and precision Higgs physics.

Dark matter models with a strongly interacting coannihilation partner have two striking features regarding relic density and collider signatures. First, the coannihilation paradigm provides an explicit counterpart to the WIMP miracle, giving weak scale masses and the correct relic density unencumbered by weak couplings or weak scale cross sections. In particular, the relic density is determined by four types of (co)annihilation channels. The DM X $\to$ SM$_1$ SM$_2$ channel dominates in the funnel region, where $m_{\mathrm{DM}} + m_{\mathrm{X}} \approx m_{\mathrm{M}}$. The DM X $\to$ M V_{SM} and $\overline{\mathrm{DM}}$ DM $\to$ M* M processes can become relevant for large DM masses, above the resonant coannihilation funnel. The $\overline{\mathrm{X}}$ X $\to \overline{\mathrm{SM}}$ SM process, since X has a color charge, efficiently annihilates X particles into quark and gluon pairs, and is most important in the low m_{DM} region. This process determines the underclosure bound on m_{DM} for a given fractional X–DM mass splitting Δ and can push the preferred dark matter mass into the multi-TeV range for $\Delta \lesssim 0.01$. For $0.1 \leq \Delta \leq 0.125$, though, the relic density motivates dark matter masses $m_{\mathrm{DM}} \sim 300$–$500\,\mathrm{GeV}$, consistent with direct and indirect detection constraints and within the current and near future reach of LHC searches.

The existence of a colored coannihilation partner and a colored mediator M ensures strong pair production of these particles at hadron colliders, and since M couples to first generation quarks, single mediator production is also possible. These production modes, when considered in tandem with the decay processes dictated by the *s*-channel coannihilation diagram, present very promising and interesting targets for LHC searches.

The conventional searches at ATLAS and CMS already provide interesting constraints on the parameter space of the model. We have seen that single dijet searches constrain a combination of the mediator width and its dark and visible couplings, which in turn

reduces the importance of the DM $X \to M \, V_{SM}$ and $\overline{DM} \, DM \to M^* \, M$ subprocesses in the relic density calculation and narrows the width of the coannihilation funnel. We have also seen that X pair production is probed in jets + MET searches, where, for $0.1 \leq \Delta \leq 0.125$, X masses below about $400 \, \text{GeV}$ are currently ruled out, and X masses around $470 \, \text{GeV}$ should be probed with $100 \, \text{fb}^{-1}$ of $13 \, \text{TeV}$ data. In addition, M pair production gives rise to a paired dijet resonance signature, where the current searches constrain M masses below $360 \, \text{GeV}$ and can potentially reach $720 \, \text{GeV}$, as long as the visible branching fraction is 100%.

Once the $M \to X$ DM decay is kinematically open, however, our proposed mediator mixed decay search pushes the mediator mass sensitivity to roughly $1 \, \text{TeV}$. This can surpass the projected reach of the jets + MET search in covering the parameter space favored by the relic density calculation. This dijet resonance plus MET signal is characteristic of many s-channel coannihilation models featuring a colored mediator. Moreover, this signature provides the only direct link between visible matter and the dark matter, and measurements of the rates and kinematics in this final state would be crucial for a determination of the dark matter Lagrangian.

Finally, we stress the intricate interplay between the relic density analysis, the fractional mass splitting parameter Δ, and the resulting reach by LHC searches, which are entirely driven the coannihilation simplified model. The minimal assumptions of the coannihilation framework [23] suffice to characterize completely the dark matter annihilation process, ensuring that the resulting collider signatures are directly motivated and driven by the potential discovery of thermal dark matter.

Acknowledgments

References

[1] PLANCK collaboration, P.A.R. Ade et al., *Planck 2015 results. XIII. Cosmological parameters*, [arXiv:1502.01589](https://arxiv.org/abs/1502.01589) [INSPIRE].

[2] PARTICLE DATA GROUP collaboration, K.A. Olive et al., *Review of Particle Physics*, [*Chin. Phys.* **C 38** (2014) 090001](https://doi.org/10.1088/1674-1137/38/9/090001) [INSPIRE].

[3] M. Beltrán, D. Hooper, E.W. Kolb, Z.A.C. Krusberg and T.M.P. Tait, *Maverick dark matter at colliders*, [*JHEP* **09** (2010) 037](https://doi.org/10.1007/JHEP09(2010)037) [arXiv:1002.4137] [INSPIRE].

[4] J. Goodman, M. Ibe, A. Rajaraman, W. Shepherd, T.M.P. Tait and H.-B. Yu, *Constraints on Light Majorana dark Matter from Colliders*, [*Phys. Lett.* **B 695** (2011) 185](https://doi.org/10.1016/j.physletb.2010.11.009) [arXiv:1005.1286] [INSPIRE].

[5] Y. Bai, P.J. Fox and R. Harnik, *The Tevatron at the Frontier of Dark Matter Direct Detection*, [*JHEP* **12** (2010) 048](https://doi.org/10.1007/JHEP12(2010)048) [arXiv:1005.3797] [INSPIRE].

[6] J. Goodman, M. Ibe, A. Rajaraman, W. Shepherd, T.M.P. Tait and H.-B. Yu, *Constraints on Dark Matter from Colliders*, [*Phys. Rev.* **D 82** (2010) 116010](https://doi.org/10.1103/PhysRevD.82.116010) [arXiv:1008.1783] [INSPIRE].

[7] C. Bartels, O. Kittel, U. Langenfeld and J. List, *Model-independent WIMP Characterisation using ISR*, [arXiv:1202.6516](https://arxiv.org/abs/1202.6516) [INSPIRE].

[8] LHC NEW PHYSICS WORKING GROUP collaboration, D. Alves, *Simplified Models for LHC New Physics Searches*, [*J. Phys.* **G 39** (2012) 105005](https://doi.org/10.1088/0954-3899/39/10/105005) [arXiv:1105.2838] [INSPIRE].

[9] H. An, L.-T. Wang and H. Zhang, *Dark matter with t-channel mediator: a simple step beyond contact interaction*, [*Phys. Rev.* **D 89** (2014) 115014](https://doi.org/10.1103/PhysRevD.89.115014) [arXiv:1308.0592] [INSPIRE].

[10] A. DiFranzo, K.I. Nagao, A. Rajaraman and T.M.P. Tait, *Simplified Models for Dark Matter Interacting with Quarks*, [*JHEP* **11** (2013) 014](https://doi.org/10.1007/JHEP11(2013)014) [*Erratum ibid.* **01** (2014) 162] [arXiv:1308.2679] [INSPIRE].

[11] A. De Simone, G.F. Giudice and A. Strumia, *Benchmarks for Dark Matter Searches at the LHC*, [*JHEP* **06** (2014) 081](https://doi.org/10.1007/JHEP06(2014)081) [arXiv:1402.6287] [INSPIRE].

[12] J. Abdallah et al., *Simplified Models for Dark Matter and Missing Energy Searches at the LHC*, [arXiv:1409.2893](https://arxiv.org/abs/1409.2893) [INSPIRE].

[13] M.R. Buckley, D. Feld and D. Goncalves, *Scalar Simplified Models for Dark Matter*, [*Phys. Rev.* **D 91** (2015) 015017](https://doi.org/10.1103/PhysRevD.91.015017) [arXiv:1410.6497] [INSPIRE].

[14] P. Harris, V.V. Khoze, M. Spannowsky and C. Williams, *Constraining Dark Sectors at Colliders: Beyond the Effective Theory Approach*, [*Phys. Rev.* **D 91** (2015) 055009](https://doi.org/10.1103/PhysRevD.91.055009) [arXiv:1411.0535] [INSPIRE].

[15] M. Garny, A. Ibarra and S. Vogl, *Signatures of Majorana dark matter with t-channel mediators*, [*Int. J. Mod. Phys.* **D 24** (2015) 1530019](https://doi.org/10.1142/S0218271815300190) [arXiv:1503.01500] [INSPIRE].

[16] J. Abdallah et al., *Simplified Models for Dark Matter Searches at the LHC*, [*Phys. Dark Univ.* **9-10** (2015) 8](https://doi.org/10.1016/j.dark.2015.08.001) [arXiv:1506.03116] [INSPIRE].

[17] CMS collaboration, *Search for dark matter, extra dimensions and unparticles in monojet events in proton-proton collisions at $\sqrt{s} = 8\,TeV$*, *Eur. Phys. J.* **C 75** (2015) 235 [arXiv:1408.3583] [INSPIRE].

[18] CMS collaboration, *Search for new phenomena in monophoton final states in proton-proton collisions at $\sqrt{s} = 8\,TeV$*, *Phys. Lett.* **B 755** (2016) 102 [arXiv:1410.8812] [INSPIRE].

[19] ATLAS collaboration, *Search for new phenomena in events with a photon and missing transverse momentum in pp collisions at $\sqrt{s} = 8\,TeV$ with the ATLAS detector*, *Phys. Rev.* **D 91** (2015) 012008 [*Erratum ibid.* **D 92** (2015) 059903] [arXiv:1411.1559] [INSPIRE].

[20] ATLAS collaboration, *Search for new phenomena in final states with an energetic jet and large missing transverse momentum in pp collisions at $\sqrt{s} = 8\,TeV$ with the ATLAS detector*, *Eur. Phys. J.* **C 75** (2015) 299 [*Erratum ibid.* **C 75** (2015) 408] [arXiv:1502.01518] [INSPIRE].

[21] CMS collaboration, *Search for dark matter with jets and missing transverse energy at $13\,TeV$*, CMS-PAS-EXO-15-003 (2015).

[22] D. Abercrombie et al., *Dark Matter Benchmark Models for Early LHC Run-2 Searches: Report of the ATLAS/CMS Dark Matter Forum*, arXiv:1507.00966 [INSPIRE].

[23] M.J. Baker et al., *The Coannihilation Codex*, *JHEP* **12** (2015) 120 [arXiv:1510.03434] [INSPIRE].

[24] K. Griest and D. Seckel, *Three exceptions in the calculation of relic abundances*, *Phys. Rev.* **D 43** (1991) 3191 [INSPIRE].

[25] G. Bertone, D. Hooper and J. Silk, *Particle dark matter: Evidence, candidates and constraints*, *Phys. Rept.* **405** (2005) 279 [hep-ph/0404175] [INSPIRE].

[26] J.L. Feng and J. Kumar, *The WIMPless Miracle: Dark-Matter Particles without Weak-Scale Masses or Weak Interactions*, *Phys. Rev. Lett.* **101** (2008) 231301 [arXiv:0803.4196] [INSPIRE].

[27] J.L. Feng, M. Kaplinghat, H. Tu and H.-B. Yu, *Hidden Charged Dark Matter*, *JCAP* **07** (2009) 004 [arXiv:0905.3039] [INSPIRE].

[28] N.F. Bell, Y. Cai and A.D. Medina, *Co-annihilating Dark Matter: Effective Operator Analysis and Collider Phenomenology*, *Phys. Rev.* **D 89** (2014) 115001 [arXiv:1311.6169] [INSPIRE].

[29] Y. Hochberg, E. Kuflik, T. Volansky and J.G. Wacker, *Mechanism for Thermal Relic Dark Matter of Strongly Interacting Massive Particles*, *Phys. Rev. Lett.* **113** (2014) 171301 [arXiv:1402.5143] [INSPIRE].

[30] E. Izaguirre, G. Krnjaic and B. Shuve, *Discovering Inelastic Thermal-Relic Dark Matter at Colliders*, *Phys. Rev.* **D 93** (2016) 063523 [arXiv:1508.03050] [INSPIRE].

[31] E. Eichten, I. Hinchliffe, K.D. Lane and C. Quigg, *Super Collider Physics*, *Rev. Mod. Phys.* **56** (1984) 579 [*Addendum ibid.* **58** (1986) 1065] [INSPIRE].

[32] A. Gupta, R. Primulando and P. Saraswat, *A New Probe of Dark Sector Dynamics at the LHC*, *JHEP* **09** (2015) 079 [arXiv:1504.01385] [INSPIRE].

[33] M. Autran, K. Bauer, T. Lin and D. Whiteson, *Searches for dark matter in events with a resonance and missing transverse energy*, *Phys. Rev.* **D 92** (2015) 035007 [arXiv:1504.01386] [INSPIRE].

[34] Y. Bai, J. Bourbeau and T. Lin, *Dark matter searches with a mono-Z′ jet*, *JHEP* **06** (2015) 205 [arXiv:1504.01395] [INSPIRE].

[35] UTFIT collaboration, M. Bona et al., *Model-independent constraints on ΔF = 2 operators and the scale of new physics*, *JHEP* **03** (2008) 049 [arXiv:0707.0636] [INSPIRE].

[36] G. Isidori, Y. Nir and G. Perez, *Flavor Physics Constraints for Physics Beyond the Standard Model*, *Ann. Rev. Nucl. Part. Sci.* **60** (2010) 355 [arXiv:1002.0900] [INSPIRE].

[37] G.F. Giudice, B. Gripaios and R. Sundrum, *Flavourful Production at Hadron Colliders*, *JHEP* **08** (2011) 055 [arXiv:1105.3161] [INSPIRE].

[38] J.M. Arnold, M. Pospelov, M. Trott and M.B. Wise, *Scalar Representations and Minimal Flavor Violation*, *JHEP* **01** (2010) 073 [arXiv:0911.2225] [INSPIRE].

[39] J.F. Gunion, H.E. Haber, G.L. Kane and S. Dawson, *The Higgs Hunter's Guide*, *Front. Phys.* **80** (2000) 1 [INSPIRE].

[40] B.A. Dobrescu, G.D. Kribs and A. Martin, *Higgs Underproduction at the LHC*, *Phys. Rev.* **D 85** (2012) 074031 [arXiv:1112.2208] [INSPIRE].

[41] K. Kumar, R. Vega-Morales and F. Yu, *Effects from New Colored States and the Higgs Portal on Gluon Fusion and Higgs Decays*, *Phys. Rev.* **D 86** (2012) 113002 [*Erratum ibid.* **D 87** (2013) 119903] [arXiv:1205.4244] [INSPIRE].

[42] CMS, ATLAS collaborations, *Measurements of the Higgs boson production and decay rates and constraints on its couplings from a combined ATLAS and CMS analysis of the LHC pp collision data at √s = 7 and 8 TeV*, CMS-PAS-HIG-15-002 (2015).

[43] A. Djouadi, *The anatomy of electro-weak symmetry breaking. II. The Higgs bosons in the minimal supersymmetric model*, *Phys. Rept.* **459** (2008) 1 [hep-ph/0503173] [INSPIRE].

[44] ATLAS collaboration, *Search for squarks and gluinos with the ATLAS detector in final states with jets and missing transverse momentum using √s = 8 TeV proton–proton collision data*, *JHEP* **09** (2014) 176 [arXiv:1405.7875] [INSPIRE].

[45] CMS collaboration, *Search for supersymmetry in the multijet and missing transverse momentum final state in pp collisions at 13 TeV*, *Phys. Lett.* **B 758** (2016) 152 [arXiv:1602.06581] [INSPIRE].

[46] ATLAS collaboration, *Search for squarks and gluinos in final states with jets and missing transverse momentum at √s = 13 TeV with the ATLAS detector*, ATLAS-CONF-2015-062 (2015).

[47] CMS collaboration, *Search for new physics in the multijet and missing transverse momentum final state in proton-proton collisions at √s = 8 TeV*, *JHEP* **06** (2014) 055 [arXiv:1402.4770] [INSPIRE].

[48] N.D. Christensen and C. Duhr, *FeynRules — Feynman rules made easy*, *Comput. Phys. Commun.* **180** (2009) 1614 [arXiv:0806.4194] [INSPIRE].

[49] A. Alloul, N.D. Christensen, C. Degrande, C. Duhr and B. Fuks, *FeynRules 2.0 — A complete toolbox for tree-level phenomenology*, *Comput. Phys. Commun.* **185** (2014) 2250 [arXiv:1310.1921] [INSPIRE].

[50] A. Kaminska and M. de Vries, *FeynRules Model Database: Simplified Models for Coannihilating Dark Matter*, https://feynrules.irmp.ucl.ac.be/wiki/SimplifiedDM.

[51] C. Degrande, C. Duhr, B. Fuks, D. Grellscheid, O. Mattelaer and T. Reiter, *UFO — The Universal FeynRules Output*, *Comput. Phys. Commun.* **183** (2012) 1201 [arXiv:1108.2040] [INSPIRE].

[52] G. Bélanger, F. Boudjema, A. Pukhov and A. Semenov, *MicrOMEGAs4.1: two dark matter candidates*, *Comput. Phys. Commun.* **192** (2015) 322 [arXiv:1407.6129] [INSPIRE].

[53] A. Belyaev, N.D. Christensen and A. Pukhov, *CalcHEP 3.4 for collider physics within and beyond the Standard Model*, *Comput. Phys. Commun.* **184** (2013) 1729 [arXiv:1207.6082] [INSPIRE].

[54] M. Backovic, K. Kong and M. McCaskey, *MadDM v.1.0: Computation of Dark Matter Relic Abundance Using MadGraph5*, *Physics of the Dark Universe* **5-6** (2014) 18 [arXiv:1308.4955] [INSPIRE].

[55] M. Backovic, A. Martini, K. Kong, O. Mattelaer and G. Mohlabeng, *MadDM: New dark matter tool in the LHC era*, *AIP Conf. Proc.* **1743** (2016) 060001 [arXiv:1509.03683] [INSPIRE].

[56] J. Alwall, M. Herquet, F. Maltoni, O. Mattelaer and T. Stelzer, *MadGraph 5: Going Beyond*, *JHEP* **06** (2011) 128 [arXiv:1106.0522] [INSPIRE].

[57] J. Alwall et al., *The automated computation of tree-level and next-to-leading order differential cross sections and their matching to parton shower simulations*, *JHEP* **07** (2014) 079 [arXiv:1405.0301] [INSPIRE].

[58] T. Sjöstrand, S. Mrenna and P.Z. Skands, *A Brief Introduction to PYTHIA 8.1*, *Comput. Phys. Commun.* **178** (2008) 852 [arXiv:0710.3820] [INSPIRE].

[59] DELPHES 3 collaboration, J. de Favereau et al., *DELPHES 3, A modular framework for fast simulation of a generic collider experiment*, *JHEP* **02** (2014) 057 [arXiv:1307.6346] [INSPIRE].

[60] M.L. Mangano, M. Moretti, F. Piccinini, R. Pittau and A.D. Polosa, *ALPGEN, a generator for hard multiparton processes in hadronic collisions*, *JHEP* **07** (2003) 001 [hep-ph/0206293] [INSPIRE].

[61] A. Ibarra, A. Pierce, N.R. Shah and S. Vogl, *Anatomy of Coannihilation with a Scalar Top Partner*, *Phys. Rev.* **D 91** (2015) 095018 [arXiv:1501.03164] [INSPIRE].

[62] B.A. Dobrescu and F. Yu, *Coupling-mass mapping of dijet peak searches*, *Phys. Rev.* **D 88** (2013) 035021 [*Erratum ibid.* **D 90** (2014) 079901] [arXiv:1306.2629] [INSPIRE].

[63] M. Chala, F. Kahlhoefer, M. McCullough, G. Nardini and K. Schmidt-Hoberg, *Constraining Dark Sectors with Monojets and Dijets*, *JHEP* **07** (2015) 089 [arXiv:1503.05916] [INSPIRE].

[64] CMS collaboration, *Search for narrow resonances in dijet final states at $\sqrt{s} = 8\,TeV$ with the novel CMS technique of data scouting*, *Phys. Rev. Lett.* **117** (2016) 031802 [arXiv:1604.08907] [INSPIRE].

[65] ATLAS collaboration, *Search for new phenomena in the dijet mass distribution using $p - p$ collision data at $\sqrt{s} = 8\,TeV$ with the ATLAS detector*, *Phys. Rev.* **D 91** (2015) 052007 [arXiv:1407.1376] [INSPIRE].

[66] UA2 collaboration, J. Alitti et al., *A search for new intermediate vector mesons and excited quarks decaying to two jets at the CERN $\bar{p}p$ collider*, *Nucl. Phys.* **B 400** (1993) 3 [INSPIRE].

[67] CDF collaboration, F. Abe et al., *Search for new particles decaying to dijets at CDF*, *Phys. Rev.* **D 55** (1997) R5263 [`hep-ex/9702004`] [ɪɴSPIRE].

[68] CDF collaboration, T. Aaltonen et al., *Search for new particles decaying into dijets in proton-antiproton collisions at* $\sqrt{s} = 1.96\,TeV$, *Phys. Rev.* **D 79** (2009) 112002 [`arXiv:0812.4036`] [ɪɴSPIRE].

[69] CMS collaboration, *Search for pair-produced dijet resonances in four-jet final states in pp collisions at* $\sqrt{s} = 7\,TeV$, *Phys. Rev. Lett.* **110** (2013) 141802 [`arXiv:1302.0531`] [ɪɴSPIRE].

[70] CMS collaboration, *Search for pair-produced resonances decaying to jet pairs in proton-proton collisions at* $\sqrt{s} = 8\,TeV$, *Phys. Lett.* **B 747** (2015) 98 [`arXiv:1412.7706`] [ɪɴSPIRE].

[71] ATLAS collaboration, *Search for pair-produced massive coloured scalars in four-jet final states with the ATLAS detector in proton-proton collisions at* $\sqrt{s} = 7\,TeV$, *Eur. Phys. J.* **C 73** (2013) 2263 [`arXiv:1210.4826`] [ɪɴSPIRE].

[72] C. Borschensky and A. Kulesza, *NLL-fast*, http://pauli.uni-muenster.de/∼akule_01/nllwiki/index.php/NLL-fast.

[73] W. Beenakker, S. Brensing, M. Krämer, A. Kulesza, E. Laenen and I. Niessen, *Soft-gluon resummation for squark and gluino hadroproduction*, *JHEP* **12** (2009) 041 [`arXiv:0909.4418`] [ɪɴSPIRE].

[74] A. Kulesza and L. Motyka, *Soft gluon resummation for the production of gluino-gluino and squark-antisquark pairs at the LHC*, *Phys. Rev.* **D 80** (2009) 095004 [`arXiv:0905.4749`] [ɪɴSPIRE].

[75] A. Kulesza and L. Motyka, *Threshold resummation for squark-antisquark and gluino-pair production at the LHC*, *Phys. Rev. Lett.* **102** (2009) 111802 [`arXiv:0807.2405`] [ɪɴSPIRE].

[76] P.M. Nadolsky et al., *Implications of CTEQ global analysis for collider observables*, *Phys. Rev.* **D 78** (2008) 013004 [`arXiv:0802.0007`] [ɪɴSPIRE].

[77] G. Salam and A. Weiler, *Collider Reach*, http://collider-reach.web.cern.ch.

[78] M. Czakon and A. Mitov, *Top++: A Program for the Calculation of the Top-Pair Cross-Section at Hadron Colliders*, *Comput. Phys. Commun.* **185** (2014) 2930 [`arXiv:1112.5675`] [ɪɴSPIRE].

[79] A. Buckley et al., *LHAPDF6: parton density access in the LHC precision era*, *Eur. Phys. J.* **C 75** (2015) 132 [`arXiv:1412.7420`] [ɪɴSPIRE].

[80] NNPDF collaboration, R.D. Ball et al., *Parton distributions for the LHC Run II*, *JHEP* **04** (2015) 040 [`arXiv:1410.8849`] [ɪɴSPIRE].

[81] M. Drees, H. Dreiner, D. Schmeier, J. Tattersall and J.S. Kim, *CheckMATE: Confronting your Favourite New Physics Model with LHC Data*, *Comput. Phys. Commun.* **187** (2015) 227 [`arXiv:1312.2591`] [ɪɴSPIRE].

[82] P. Nath and A.B. Spisak, *Gluino Coannihilation and Observability of Gluinos at LHC RUN II*, *Phys. Rev.* **D 93** (2016) 095023 [`arXiv:1603.04854`] [ɪɴSPIRE].

[83] A. Delgado, A. Martin and N. Raj, *Extending the Reach of Compressed Gluinos at the LHC*, `arXiv:1605.06479` [ɪɴSPIRE].

[84] M. Cacciari, G.P. Salam and G. Soyez, *The anti-k(t) jet clustering algorithm*, *JHEP* **04** (2008) 063 [`arXiv:0802.1189`] [ɪɴSPIRE].

[85] A. Avetisyan et al., *Methods and Results for Standard Model Event Generation at* $\sqrt{s} = 14\,TeV$, $33\,TeV$ and $100\,TeV$ *Proton Colliders (A Snowmass Whitepaper)*, arXiv:1308.1636 [INSPIRE].

[86] W. Beenakker et al., *NLO+NLL squark and gluino production cross-sections with threshold-improved parton distributions*, *Eur. Phys. J.* **C 76** (2016) 53 [arXiv:1510.00375] [INSPIRE].

[87] J.M. Campbell and R.K. Ellis, *MCFM for the Tevatron and the LHC*, *Nucl. Phys. Proc. Suppl.* **205-206** (2010) 10 [arXiv:1007.3492] [INSPIRE].

[88] S.D. Ellis, Z. Kunszt and D.E. Soper, *Two jet production in hadron collisions at order* α_s^3 *in QCD*, *Phys. Rev. Lett.* **69** (1992) 1496 [INSPIRE].

[89] W.T. Giele, E.W.N. Glover and D.A. Kosower, *The Two-Jet Differential Cross section at* $\mathcal{O}(\alpha_s^3)$ *in Hadron Collisions*, *Phys. Rev. Lett.* **73** (1994) 2019 [hep-ph/9403347] [INSPIRE].

[90] ATLAS collaboration, *Expected performance of the ATLAS b-tagging algorithms in Run-2*, ATL-PHYS-PUB-2015-022 (2015).

[91] J. Gaiser, *Charmonium Spectroscopy From Radiative Decays of the* J/ψ *and* ψ', Ph.D. Thesis, SLAC (1982).